Improving the detection of shell alteration: Implications for sclerochronology

Coimbra, Rute; Huck, Stefan; de Winter, Niels J.; Heimhofer, Ulrich; Claeys, Philippe

Published in:
Palaeogeography, Palaeoclimatology, Palaeoecology

DOI:
10.1016/j.palaeo.2020.109968

Publication date:
2020

Improving the detection of shell alteration: implications for sclerochronology

Rute Coimbra[a*], Stefan Huck[b], Niels J. de Winter[c,d], Ulrich Heimhofer[b], Philippe Claeys[c]

a) GeoBioTec, Departamento de Geociências, Universidade de Aveiro, Portugal
b) Institut für Geologie, Leibniz Universität Hannover, Germany
c) Analytical, Environmental and Geochemistry Department, Vrije Universiteit Brussel, Pleinlaan 2, 1050 Brussels, Belgium
d) Stratigraphy and Paleontology group, Faculty of Geosciences, Utrecht University, the Netherlands

*Corresponding author: Rute Coimbra (rcoimbra@ua.pt)

Dpto. Geociências, Universidade de Aveiro

Campus de Santiago, 3810-193 Aveiro, Portugal

+351 234 370357

Co-authors: huck@geowi.uni-hannover.de; niels.de.winter@vub.be ; heimhofer@geowi.uni-hannover.de; phclaeys@vub.be

Keywords: Shells, geochemistry, diagenesis, statistical analysis, paleoenvironment

Abstract

Sclerochronology makes use of valuable (fossil) shell-archives to establish records allowing for investigation of high-resolution environmental dynamics. Nevertheless, this potential can often not be fully exploited due to the interplay between paleoenvironmental variability, vital effects and the potential diagenetic modification of skeletal materials, which often results in highly complex records. A novel dynamic method, aiming to separate pristine from altered shell material for paleoclimate and paleoenvironmental reconstructions is proposed.

Seventeen fossil bivalve shells (requieniid rudists, pectinids and chondrodonts) from two neighbouring Lower Cretaceous (Albian) shallow-water sections (Lusitanian Basin, western Portugal) were analysed for their major and trace elemental compositions using high-resolution quantitative μXRF line scans. Their complex records were subject to a novel statistical analysis protocol, which tested mono- and multi-species datasets, as well as comparing shells from both locations.

Characteristic elemental associations revealed the differential impact of early to late diagenetic alteration processes. The incorporation of elements associated with detrital contribution (Fe, Si, Al) is attributed to syn-depositional bioerosion (shell-boring). In clear contrast, shell-portions showing a strong correlation between Fe and Mn are indicative of later diagenetic alteration. The influence of each process was different at each site, revealing local differential alteration pathways. Mono-specific comparisons provided identical geochemical responses, suggesting that intra-specific differences are not dominant for the observed elemental patters. In contrast, inter-species tests rendered a clear separation in the way elements are incorporated in the shells of pectinids and requieniids (e.g., as evidenced by differences in Sr content). Such differences can be linked to differential biomineralization mechanisms, easily detected by the applied method.

We present a new, dynamic method for distinguishing pristine from altered shell material, not relying on arbitrary diagenetic thresholds for trace element content. By clearly identifying shell-alteration pathways, syn- to post-depositional processes were recognized. A progressive cleaning of the elemental dataset allows paleoenvironmental studies to be based on the most pristine data, contributing to unravel the complex interplay between climate, environmental dynamics and their impact on biomineralization processes and sclerochronological archives.

1- Introduction

The study of past climate and environmental change yields crucial information about Earth's climate system and how global perturbations can affect the biosphere (e.g. Grice et al., 2005; Zachos et al., 2001; Gingerich, 2006). Most of these studies aim to characterize perturbations on a geological time scale (thousands to millions of years), identifying long term trends in climate, environment and ecology. Contrarily, the field of sclerochronology uses mineral, structural and chemical changes in accretionary biogenic archives to study changes in environment that take place on the scale of lifespans of the animals (e.g. several years) that form these archives (e.g. Jones, 1983). These studies complement longer timescale reconstructions and have the potential to yield snapshots of climate and environmental variability on a shorter timescale which can be placed in the context of larger timescale perturbations (e.g. Steuber et al., 2005). Bivalve shells have been an especially popular archive for sclerochronology work, because their growth rates are comparatively high (reported values ranging from 20 mm/yr to 4 cm/yr in extreme conditions; e.g. Batenburg et al., 2012; Schöne et al., 2005; Nedoncelle et al., 2013) and because the calcite shells of some species of bivalves (e.g. oysters and pectinids) are more resistant to diagenesis than their aragonitic counterparts (e.g. corals and gastropods; e.g. Brand and Veizer, 1980; 1981).

In addition, growth lines and increments in the shells of bivalves have been successfully applied to construct independent shell chronologies which allow researchers to accurately assess the timing of shell formation and link shell chemistry to environmental variability in modern species (e.g. Richardson et al., 2004; Schöne et al., 2005; Gillikin et al., 2008). However, the complex interplay of multiple environmental, physiological and post depositional (diagenetic) parameters on the chemical composition of bivalve shells has hampered the interpretation of the above mentioned chemical variations in terms of environmental change. As a result, sclerochronologists often combine several chemical tracers in a multi-proxy approach in an attempt to disentangle the effects of different parameters on shell composition (e.g. Surge et al., 2001; de Winter et al., 2017; 2018).

Concerning the specific case of elemental records obtained from biogenic calcite and/or aragonite, these have been used to reconstruct (paleo) environmental parameters (temperature, salinity, primary productivity, current patterns; e.g. Nürnberg et al., 1996; Halfar et al., 2000; Surge et al., 2001; Gillikin et al., 2008; Chan et al., 2011; Schöne et al., 2011; de Winter et al., 2017; 2018; Ullmann et al., 2018; Huyghe et al., 2019; Markulin et al., 2019). Nevertheless, strong differences in calcification mechanim are often found to disrupt an already naturally complex signal, further hampered by the effects of diagenesis in fossil shell materials. The cautious use of statistic tools provides a valuable solution for this limitation.

Principal component analysis (PCA) is among the most popular multivariate statistical techniques for dealing with such large datasets, and is widely used across many scientific disciplines (Cordella, 2012; Yao et al., 2012; Coimbra et al., 2015, 2018; Cai et al., 2019). PCA aims to extract, compress, simplify and analyse the structure of multivariate datasets. Based on observations of several dependent variables, their inter-correlation is tested and expressed as a set of new orthogonal variables (Principal Components- PC), evidencing the degree of similarity between observations and variables (Abdi and Williams, 2010 and references therein). In this study, as an innovative approach to sclerochronological data, a double PCA approach is applied (Coimbra et al., 2017), with a new automated adaptation (density analysis) for higher precision in isolating samples of interest.

The proposed data reduction approaches simplify the evaluation of elemental variations in shell archives, highlighting taxon and habitat specific variations in trace element content. Environmental and diagenetic influence on original elemental composition can be addressed efficiently, allowing the identification of growth rhythms or responses of shell microstructure. This contribution provides significant advances in the detection of shell-alteration, with the potential of refining sclerochronological interpretations for a variety of skeletal remains from a wide range of geological time periods.

2- Geological and paleoenvironmental setting

The well-exposed sections at São Julião (38.9319776ºN, 9.4219073ºW) and Praia das Maçãs (38.8297059ºN, 9.468163ºW) are located along the western coast of Portugal, within the southern sector of the Lusitanian Basin (Figs. 1 and 2). During the Cretaceous, the western Iberian plate was located at about 30ºN (Stampfli and Borel, 2002), under the influence of two major climatic zones: the mid-latitude warm humid belt and the northern hot arid belt (Chumakov et al., 1995). Throughout the Lusitanian Basin, a major unconformity marks the Aptian-Albian transition (Dinis and Trincão, 1995; Heimhofer et al., 2007; Dinis et al., 2008). This regional unconformity is overlain by coarse-grained siliciclastics (Rodízio Formation) deposited diachronously throughout the basin in fluvial-deltaic settings. These deposits are covered by nearshore marine deposits and shallow-water carbonate platforms of the Galé Formation of Albian age. The deposits are overlain by lagoonal and terrestrial deposits– the Caneças Formation.

The studied sedimentary successions comprise shallow-water carbonate-siliciclastic deposits (Figs. 2 and 3), assigned by previous workers to cover Albian to Early Cenomanian age (Rodízio and Galé Formations; Hasenboehler, 1981; Medus, 1982; Berthou, 1984; Rey, 1992; Horikx et al., 2014). The Albian Galé Formation is subdivided into the Água Doce Member and the Ponta da Galé Member (Rey, 1992). The lowermost Água Doce Member is mainly composed of alternating marly, carbonate- and sandstone-rich coastal-marine deposits. More marine conditions are evidenced by increasingly thicker limestone beds towards the top of this member and mark the transition to the overlying carbonate-rich Ponta da Galé Member (Rey 1992). This work will focus on the stratigraphic interval covering the Ponta da Galé Member—the carbonate-rich upper portion of the Galé Formation, which is defined by the regional occurrence of the first rudist beds, evidencing an overall deepening trend (Rey, 1992). An overview of the main sedimentological, stratigraphical, and paleontological features of the São Julião and Praia das Maçãs sections is given in Fig. 3A. Based on previous work performed on these sections, the stratigraphic intervals under scope are well-known for not having experienced pervasive deep-diagenetic influence (Horikx et al. 2014, 2016; Coimbra et al., 2017), justifying their use for exploring sclerochronological aspects. The regional correlation between both has been well-established using C-isotope stratigraphy, here partially reproduced after Horikx et al. (2014) (Fig. 3A). Accordingly, the base of the Praia das Maçãs section can be correlated to the second rudist-bearing bed at Sao Julião (165 m; Fig. 3A). Both sections are characterised by decreasing trend in C isotopes bottom to top, despite minor differences in absolute value. Shells retrieved from these deposits (examples in Fig. 3B) are investigated to explore the potential and evaluate the limitations of these shells as archives of paleoenvironmental change.

3- Studied shell materials

3.1- *Pectinidae*

Nowadays, bivalves belonging to the superfamily Pectinidae Rafinesque, 1815 (scallops) occupy a huge variety of habitats in polar, temperate and tropical seas, ranging from the intertidal zone to water depths up to 7000 m (Brand, 2006; Serb, 2006). They can be byssally attached, free-living or cemented; their life habit changes ontogenetically (Stanley, 1970). Largely, ancient pectinid shells such as those of *Amussiopecten baranensis* comprise an outer layer composed of (crossed, regular or irregular) foliated low-Mg calcite (LMC), a middle aragonitic layer and an inner foliated LMC layer (Zamarreño et al., 1996; Carter 1990). Commonly, shells of Cretaceous pectinids such as *Prohinnites favrinus* are predominantly composed of foliated calcite (Harper et al., 1996). The inner crossed-lamellar aragonite layers of these shells are often replaced by coarse, sparry low-Mg calcite (Harper et al., 1996).

3.2- Rudists

Rudist bivalves (superfamily Hippuritoidea) are epibenthic sessile suspension-feeders that inhabited a variety of carbonate-dominated shallow water settings in the (sub-) tropical Tethyan-Atlantic-Pacific ocean belt during late Mesozoic times (Gili et al., 1995; Skelton, 2003; Skelton, 2018; Gili and Götz, 2018). During the Cretaceous, they evolved to one of the most important neritic carbonate producers, with maximum carbonate production rates ranging between 2.2 and 35.7 kg per square meter per year (Steuber, 2000). In contrast to reef-building corals, rudists were typically loosely arranged in low-relief bioconstructions referred to as bouquets (n <12), clusters (n= >12) or thickets (n= >100; Philip, 1972; Gili et al., 1995). Significant differences in growth geometries (morphotypes) indicate that rudists were able to adapt to various habitats. Recumbent forms lay prone but unattached on mobile substrates in current-swept settings (Ross and Skelton, 1993). In contrast, the left valve of so-called ‘clingers’ was attached (cemented) to solid substrates (Skelton, 1978). During ontogeny, the elongated and initially cemented valve of predominantly cylindrical ‘elevators’ stabilized by surrounding sediment or by neighbouring rudists (clustering; Gili and Götz, 2018).

In general, the shell of rudists comprises two layers: a rarely preserved inner layer originally composed of crossed lamellar aragonite and an outer low-Mg calcite layer composed of fibrous prisms (Skelton and Smith, 2000; Skelton, 2018). The mesostructural properties of the outer layer, however, show significant differences among the rudist families (Skelton, 2018). Whereas Hippuritidae and Requieniidae provide relatively compact and thick calcitic shells, the right valves of most Radiolitidae typically shows a complex celluloprismatic structure composed of numerous cells, often spar-filled after fossilization (Pons and Vicens, 2008).

4. Methods

4.1- Sample collection and preparation

Shells collected during field work were cut to obtain thin sections and polished surfaces (Fig A1 for high-resolution images of all studied specimens). Selected shells were embedded in resin (Araldite® 2020, Huntsman, Basel, Switzerland) and subsequently cut along their major growth axis using a slow rotating rotary saw. A parallel slab was cut out of one-half of the shell, while the other half was preserved (archive half). For micro-XRF scanning, slabs were polished using silicon carbide polishing discs (up to P2400).

4.2- Micro X-Ray Fluorescence

All polished shell surfaces were subject to non-destructive trace elemental analyses by means of micro-X-ray Fluorescence (micro-XRF). Analyses were carried out on a Bruker M4 Tornado micro-XRF scanner (Bruker nano GmbH, Berlin, Germany) at the AMGC research group of the Vrije Universiteit Brussel (VUB, Brussels, Belgium). The Bruker M4 Tornado is equipped with a Rh metal-ceramic X-ray source operated at maximum energy settings (50 kV, 600 µA). The X-ray beam was focused on a 25 µm diameter circular spot (calibrated for Mo-Kα radiation) and the intensity of returning X-rays was measured using two silicon drift detectors (see de Winter and Claeys, 2016). The sample position was controlled by a high-precision (±1µm) XYZ sample stage that can be moved relative to the focused X-ray beam. Details on the setup and methodology of the M4 Tornado XRF scanner can be found in de Winter and Claeys (2016) and de Winter et al. (2017). Two types of analyses were carried out: semi-quantitative elemental mapping and quantitative point-by-point line scanning.

Elemental mapping was carried out by stitching together horizontal line scans that were produced by moving the sample through the focused X-ray beam in continuous motion, using short acquisition times per 25 µm wide spot (20 ms). This acquisition time is insufficient for full quantitative analyses of individual points. Therefore, 2D-grids of relative trace element abundance were constructed by integrating the intensity under element X-ray fluorescence peaks and plotting differences in XRF intensity over the entire sample surface. These maps serve as a qualitative assessment of the nature of the material, guiding the position of quantitative XRF line scans (Fig. 4B to G). In this way, the exact path to follow during line scans was established ensuring minimal contribution of heavily altered shell portions (Fig. 4D and H).

Quantitative point-by-point micro-XRF line scans were carried out using longer integration times (60 s per point). Contrary to map analyses, line scans were carried out point by point rather than by means of continuous scanning. This approach allows the X-ray beam to stay on the same spot for enough time to reduce the signal to noise ratio of the XRF spectrum sufficiently for point-by-point quantification. The minimum time required for quantitative point analyses was determined by repeated analyses of carbonate reference materials following the protocol detailed in de Winter et al. (2017). Spectra were quantified using the Bruker Esprit software calibrated using the matrix-matched BAS-CRM393 limestone standard (Bureau of Analyzed samples, Middlesbrough, UK), after which individual measurements were calibrated offline using seven matrix-matched international certified reference materials (CCH1, COQ1, CRM393, CRM512, CRM513, ECRM782, and SRM1d; see de Winter et al., 2018 for details), which were treated as samples. Untreated trace element results are reported in Data_Appendix. The applied set of standards collectively contained enough certified values to allow concentrations to be quantified (calibration line R^2>0.98) for the elements Mg, Al, Si, K, Ca, Ti, Cr, Mn, Fe, Cu, Sr, Y and Ba. Other elements with less well constrained calibration lines (R^2 values between 0.9 and 0.98) include P, Zn, Zr, Nb and Pb. These elements are more difficult to quantify because their XRF peaks tend to overlap with elements which are more common in bivalve carbonate (see de Winter and Claeys, 2016). These latter elements did not meet strict standards for quantification, but their semi-quantitative results can still be used to assess relative differences in elemental composition using the proposed double PCA and density analysis method.

4.3- Statistical analysis: the double PCA+ approach

The double Principal Component Analysis has proven to be useful in shallow-marine contexts (Coimbra et al., 2017; details in Appendix). In order to determine the selection of elements to include in the analysis, an exploratory PCA is performed in order to detect the most significant (loadings <-0.5 and >0.5) geochemical variables for each considered dataset (see Fig. A2 in Appendix). This ensures that the following double PCA method is carried out exclusively for the variables showing higher degree of affinity, using the statistical software package XLSAT, an add-in to Excel. Here it is adapted to process the dense sclerochronological elemental datasets produced by micro-XRF in order to provide clues on the processes acting upon these mid-Cretaceous shells during their lifetime and after deposition. We expand the double PCA method by adding density analysis—an automated criterion for accurately delimiting different clusters of samples within a dataset (see Fig. A2 in Appendix for stepwise description and Figs. A3 and A4 in for further recommendations). This improved version—double PCA+—can be applied to various combinations of datasets (one shell-transect, several transects, several sites, etc). The information generated by the double PCA+ is threefold: (i) it explores the array of possible mechanisms accounting for shell-alteration; (ii) provides arguments to isolate the best-preserved data, unlocking masked paleoenvironmental fluctuations; (iii) provides customized thresholds of shell-preservation, highlighting particularities of given sites or species. As the complete dataset comprises several geochemical variables extracted from seventeen shells belonging to two localities, the possibilities for comparison are endless. The reasoning followed during this work was to select sets of specimens suitable to perform mono-specific and multi-species analysis for each location; followed by mono-specific analysis comparing both locations. Any other selection would be equally valid, depending on the final goal (e.g., targeting specific elements of interest; ancient specimens with better constrained ecological requirements; ancient versus modern examples; modern examples only).

5- Results

5.1- The more conventional approach

The large volume of information gathered during this research surpassed 200.000 elemental values. The conventional approach of plotting the elemental data against shell length (example given in Fig. 5) can only be used when comparing a low number of transects among each other, otherwise plots become too large and chaotic. For the pectinid shells, the range of absolute values was different, as evidenced by need of different vertical scales in Fig. 5. For example, baseline Mn values for the pectinid specimen from Praia das Maçãs are much higher than those obtained for the São Julião specimen, as well as the maximum peak values. This also holds true for all other presented proxies. The temporal trends are hard to deduce due to frequent disruptions by sharp maximum peak values (noted in Fig. 5). Portions of shell with persistently high or low elemental values are also present (e.g., high Sr values in Fig. 5). Therefore, to achieve the goal of comparing the 17 specimens under scope, an alternative data-reduction method was required—the double PCA+ (see Appendix). The approach of separating the available data into sets of shells by site and/or species was chosen in order to avoid a dense cloud of overlapping data points of diverse nature, very dense and less informative.

5.2- Praia das Maçãs: mono-specific versus multi-species

For the locality of Praia das Maçãs, two groups of specimens were tested. The first group is mono-specific (Fig. 6A), with six (taxonomically undifferentiated) requiniid shells showing tightly clustered data, without evidence of major differences in elemental content. This clustering of samples forms a high-density area in the PCA-space (Fig. 6A), including 65% of the samples included in this group of shells. These were then used to establish the customized elemental threshold values of the most significant elemental proxies (see Fig. 6A and Appendix for detailed workflow). A rather large number of samples (35% of the total) fall out of this main cluster, largely following a common trend towards higher Fe, Mn and Mg content (Fig. 6A, see also Fig. A5). In fact, these samples even seem to form a smaller cluster in the density plot. Only a very small group of samples does not follow this trend, plotting towards higher Si and S abundance (lowermost portion of the PCA space, Figs. 6A and A5).

The second set of samples from Praia das Maçãs is composed of 7 shells belonging to 4 different species (Chondrodont, Hippuritid elevator rudist, pectinid and radiolitid; Figs. 6B and A4). A main data density area is defined by 85% of the samples of this group, leading to a tight cluster despite the presence of different species. Only a minority of samples plot towards negative values of PC1, in response to higher concentration of Fe, Mn and Mg; and towards the more positive range of PC2 pointing at higher abundances of Si. When considering the sample distribution per specimen, the elevator rudist and pectinid shells are both slightly shifted towards an area denoting higher Sr content. Additionally, the pectinid shell presents more samples responsible for the trend towards higher Si values.

When considering both sets of samples (mono- and multi-species), no major differences in elemental trends were observed (Figs. 6 and A5 in Appendix). Nevertheless, it is noteworthy that the mono-specific set denoted more variability in Fe, Mn and Mg (PC1 in Fig. 6A) as well as Si (PC2 in Fig. 6A); whilst the multi-species group revealed slight differences in Sr content, but overall good agreement in elemental abundance of the measured proxies (Fig. 6B).

5.3- São Julião: mono-specific versus multi-species

Specimens from the São Julião section were initially tested as a multi-species group including two *Apricardia* (*carentonensis*) shells and two pectinid shells (Figs. 7 and A5 in Appendix). The double PCA+ provided two clearly differentiated clusters defined by both species, largely attributable to significant differences in Sr and Pb content (Fig. 7A). In fact, by applying the density analysis criteria, the selected set of samples was largely composed of datapoints belonging to pectinid shells (ca. 78%), imposing an unwanted bias to this analysis. A mono-specific analysis was therefore preferred for these shells.

The dataset was consequently divided into two mono-specific sets: two *Apricardia* shells (Fig. 7B) and two pectinid shells (Fig. 7C). The *Apricardia* shells clustered tightly within a high-density area comprising ca. 80% of the samples. This set of samples was used to establish the elemental thresholds for this setting and species. Samples showing a clear trend towards lowered Ca abundance, along with higher Mg, Fe and Al content (PC1; Fig. 7B) fall out of the main cluster. Only a minor number of samples revealed the influence of trace Br and P concentration, showing an opposite trend (PC2; Fig. 7B). The two pectinid shells revealed a similar elemental profile when compared to *Apricardia* specimens: a main cluster generated by 65% of the samples, disrupted by samples denoting higher Mg, Fe, Si and S across PC1; and less significant incorporation of trace elements as Pb, Br and Zn (Fig. 7C).

5.4- São Julião versus Praia das Maçãs

Two pectinid shells retrieved at each of the studied sites were compared using the double PCA+ protocol (Figs. 8 and A5 as Appendix). Samples from both shells form a high-density cluster containing 80% of the total dataset, but samples from São Julião clearly dominate this accumulation (Fig. 8). This pattern is due to the higher dispersion evidenced by samples from the Praia das Maçãs, denoting a clear trend towards higher Mg, Fe, Mn and Br (PC1), along with lower Sr abundance (PC2). An alternative minor trend is also observed in pectinid data from Praia das Maçãs, with a small set of samples responding to higher Si (and P) content (Fig. 8).

6- Discussion

In general, the PCA results are characterized by a high number of samples clustering tightly in all cases. As such, on average 75% of the total tested samples revealed a higher data density (see Fig. A2c in Appendix), forming a main cluster (Figs. 6 to 8 and Fig. A5 as Appendix). In contrast, a small number of samples depart from this main cluster, forming different dispersion patterns (Figs. 6 to 8 and Table 1). Accordingly, the main cluster corresponds to the best-preserved samples, as evidenced by their low content in elements known to respond to diagenesis (e.g., Mn, Fe; Brand and Veizer, 1980; Al-Aasm and Veizer, 1986b). This cluster contains highly relevant information and can thus be used in terms of paleoenvironmental record. Contrarily, samples scattering away from the main cluster correspond therefore to secondary processes (alteration) that occurred at any given state of the evolution of these biogenic materials. Persistent patterns of sample distribution were identified in the sets of tested shells (Figs. 6 to 8; summarized in Fig. 9). These patterns may respond to a wide array of variables, including vital effects, paleoenvironmental conditions and syn- to post-depositional alteration. Obtained geochemical profiles can be interpreted in terms of species-dependence, site-specific processes and general disruption of the original signals; and the potential for isolating noise from paleoenvironmental information (Fig. 10). As an example of the benefits resulting from the Double PCA+ approach, Sr elemental values are addressed in Figure 11. The unprocessed raw dataset obtained for the set of mono-specific set of six Requiniiid shells (see also Figs. 3 and A1) shows sharp variations, largely towards very low abundance values (minimum value of 50 ppm; Fig. 11A). The dynamic elemental threshold values of 1204 to 1852 ppm obtained by the Double PCA+ approach (Figs. 6 and 12; Table 1) provided a range of best-preserved datapoints, representing 80% of the unprocessed data. By applying this result, the resulting Sr plots for each shell now show a clearer variation patterns, denoting certain cyclicity in the sclerochronological record (Fig. 11B). The focus of this study is to improve the detection of shell alteration, hence the significance of short-term (seasonal/ontogenetic) elemental fluctuations enclosed in the "clean" sclerocronological record are beyond the scope of this contribution.

6.1- Main geochemical trends: processes and elemental responses

At Praia das Maçãs, both intra and inter-species datasets provided similar PCA patterns (Figs. 6 and 9A). Samples deviating towards the PCA region denoting higher Fe, Mn and Mg abundance (average values in Fig. 6) are interpreted as diagenetically compromised, recrystallized shell-portions (examples in Fig. 4A and E). Fe and Mn are typically enriched in calcite during diagenesis due to their solubility and high distribution coefficients (Veizer, 1983; Rimstidt et al., 1998; Swart, 2015). Accompanying the described Fe and Mn enrichment, Mg abundance also increases in these samples, with absolute values still within LMC range (<4000 ppm; Fig. 6A). This reflects the loss of biogenic signature of the analysed calcite samples, originally leaner Mg calcite portions of the shell (ca. 2500 ppm Mg; Fig. 6A and also chapter 3), consequently also losing Sr (and Ca) during the recrystallization process (Brand and Veizer, 1980; Al-Aasm and Veizer, 1982, 1986). These interpretations are based on the combined elemental features, more informative than reading isolated elemental values. The few samples deviating towards higher Si (and S) are interpreted as the result of the incorporation of siliciclastic material (pyrite not excluded) in borings by epifaunal organisms (Fig. 4A and B). The portions of the record remaining after the double PCA+ approach can then be interpreted in terms of environmental change. The double PCA+ provides therefore solid elemental threshold values (Fig. 6). When comparing intra and inter-species PCA results, most altered samples arise from the PCA protocol performed to the set of six requiniid shells (Fig. 6A). This effect is due to the higher degree of similarity between the elemental records of each shell within a mono-specific dataset, yielding higher-density data distribution along PCA plots (see Fig. A2c for details). This trend translates into narrower threshold values. In contrast, inter-species datasets generate lower density data distribution due to generation of more diffuse main clusters (example in Fig. 6B). For the latter, it also becomes evident that within the best-preserved data, certain species have higher Sr content (ca. 1500 versus 1200 ppm; Fig. 6B), as is the case of pectinid and radiolitid shells (Fig. 6B). This effect likely relates to a differential incorporation of Sr during shell growth and/or differences in shell microstructure (and microporosity), as all these specimens belong to the same site and geological time interval and were therefore subject to similar diagenetic history (Fig. 3A). A species-dependent process may be envisaged, suggesting main differences in growth rate and/or calcification rate controlled Sr incorporation. The proposed calcification rate control on Sr operates in modern skeletal materials (Stoll and Schrag, 2000; Stoll et al., 2002; Rickaby et al., 2002; Carré et al., 2016), as well as in inorganic calcite (Lorens, 1981; Tesoriero and Pankow, 1996). Under higher calcification rates, Sr uptake occurs under kinetic control such that the animal cannot discriminate effectively against Sr, resulting in a higher distribution coefficient for this element—D_{Sr} (Elderfield et al., 2002). The reported ontogenetic decrease in growth rates for rudists (Steuber, 1996) and oysters (Ullmann et al., 2010) supports the notion that shell-growth influences Sr incorporation.

At the São Julião section, inter-species differences were larger than in Praia das Maçãs, generating a clear separation between *Apricardia* and pectinid specimens (Fig. 7A). It is noteworthy that pectinid shells, at this different location, also show a distinctive Sr signature (Fig. 7A). The most distinctive trait between *Apricardia* and pectinid shells is the concentration in Sr, on average 350 ppm higher in *Apricardia* shells (1578 versus 1226 ppm). This feature supports the previous notion that ontogenic and/or metabolic control has a strong influence on Sr incorporation. When species are analysed separately, similar PCA patterns are found (Fig. 7B and C, see also Fig. 9B), with shell-alteration characterized by elevated concentration of the elemental association of Si, Fe, Al and Mg attributed to the influence of detrital siliciclastics included in bore holes (quartz and aluminosilicate minerals). Despite well-known difficulties related to the measurement of heavy metals with XRF, the minor incorporation of heavy metals (Pb, Zn) and Br is nevertheless relevant in both species (Fig. 7B, C), in part also related to an inverse trend of decreasing phosphorous abundance (Fig. 9B). Cautious comparison with modern examples may shed light into this trend. Bioaccumulation of naturally present trace elements is a well-known process in modern settings, of extreme relevance in the context of anthropogenic contamination on coastal areas and related mitigation efforts (Ferreira et al., 2004; Du et al., 2011;

Markulin et al., 2019; VanPlantinga and Grossman, 2019). This process is of major concern regarding the soft tissue of bivalves (potentially for human consumption), but also affecting shell components. Primarily, the calcified layer of the shells is composed of a mineral phase, constituting over 95% of the shell mass. The remainder is the organic matrix (chitin, silk fibroin protein and acidic macromolecules) present as a thin envelope or sheet surrounding each mineral unit (Gregoire, 1972 in Heuer et al., 2002; Furuhashi et al., 2009). Intra-crystalline proteins occluded in the mineral lattice can also occur, potentially distorting the mineral lattice (Pokroy et al., 2006). This structure provides structural support, exerting control over the mineralization process (Jacob et al., 2009; Immenhauser et al., 2018). Proteins and carbohydrates have high affinity for heavy metals (Jacob et al., 2009), which can be remobilized during organic matrix degradation of ancient shells. Heavy metal and Br enrichment via the diagenetic stabilization of organic components can potentially explain the presence of the persistent PCA trend observed on ancient shells of different species (Fig. 7B and C and Fig. 9B).

By combining data from the same species (pectinid shells) at different locations (Praia das Maças and São Julião), a combination of all the above processes becomes apparent (Fig. 8). The specimen from Praia das Maçãs shows clear evidence of more significant late diagenetic alteration, with more samples deviating towards the PCA space corresponding to higher Mn and Fe concentration. Significant shell-boring evidence (higher Al, Si values) is also detected at this location (Fig. 8). This result may hint at higher prevalence of syn-depositional bioerosion at Praia das Maçãs compared to São Julião and highlights the potential of the double PCA+ method for highlighting changes in paleoenvironment and –ecology. Conversely, the specimen collected at São

Julião shows a tighter cluster along the PCA space, with only a few samples deviating from the main group of samples.

From all the tested shell combinations, three main patterns of sample distribution were identified on the PCA plots (Fig. 9C to E). When dealing with mono-species analysis, altered samples deviate from a main cluster, responding differently to a variety of processes (Fig. 9C). For analysis including different species, two possibilities arise: there are no evident elemental differences between species, forming one single main cluster and altered samples respond similarly (Fig. 9D); or inter-species elemental incorporation is significantly different, generating more than one main cluster from which altered samples deviate (Fig. 9E). In a next step, separate analysis (per species) is recommended (as described in Fig. 7).

6.2- Disruption of background signal

Raw elemental data corresponding to single shell transects (e.g., Fig. 5) typically present baseline values corresponding to environmentally relevant information, but often masked by noise. These interruptions of the background signal may relate to intervals of several consecutive samples showing moderately higher or lower values in respect to the baseline (Fig. 10A; trend1); or to sharp peaks generated by a small number of samples presenting higher/lower values regarding the baseline (Fig 10A; trend2). In the first case, recrystallized portions of the measured transects (e.g., cemented veinlets; Fig. 4A and E) are often the cause for this effect and the double PCA+ approach is effective in separating syn to post-depositional processes from the primary elemental signals (Fig. 10B). In the case of conspicuous peaks, corresponding to the elemental signal of small fractures and/or borings (Fig. 4A) or even instrumental noise, the impact of such a small number of samples on the overall trend is minimal, easily corrected when smoothing the paleoenvironmental data obtained after the double PCA+ (Fig. 10C).

6.3- Dynamic thresholds: filtering-out altered elemental signals

Commonly, elemental cut-off values—range of values considered for well-preserved ancient materials— are obtained from previous cases discussed in the literature (e.g. Brand and Veizer, 1980, 1981; Al-Aasm and Veizer, 1986a; b), based on well-preserved specimens tested by a wide array of techniques (petrographic inspection, geochemistry and others) and contrasted with closely related modern specimens (when available). Valuable paleoclimatic interpretations have also been produced by more sophisticated approaches (Jones et al., 2009; de Winter et al., 2017; 2018). For the present case of Cretaceous rudists, early contributions by Al-Aasm and Veizer (1986a; b) and Steuber (1996) form the backbone of sclerochronological research on these materials. For a better detection of shell-alteration, the threshold values in this study (Fig. 12 and Table 1) were obtained by performing the double PCA+ approach and confidently excluding altered samples from paleoenvironmental considerations. Applying these dynamic thresholds resulted in an average of 75% of the initial datasets for each specimen being preserved (Figs. 6 to 8 and A5), a good indication of the careful selection of specimens and overall good preservation state. When compared to available literature of coeval examples (Steuber et al., 1999; Steuber, 2000; Tibljaš et al., 2004; Damas-Mollá et al., 2006; Higuera et al., 2007), no major differences were detected in terms of the elemental range of well-preserved shell-portions (Fig. 12 and Table 1). More interestingly, traditionally used cut-off values were improved by using the case-sensitive approach—the double PCA+. This was the case for most of the most used elemental thresholds, in general narrower than literature values (Fig. 12 and Table 1).

Additionally, because these are dynamic thresholds, based on each specific case under scope, they can be applied to different sets of shells, adapting to other goals not addressed in this contribution (e.g., targeting a specific element on different shells, among a wide array of possibilities). This means that each time the Double PCA+ is applied, different thresholds can be derived, hence the designation of "dynamic" elemental thresholds. Also, they are applicable to other biogenic archives (belemnites, oysters, corals, and many others). The application of the double PCA+ allows researchers to work with more unconventional elemental data (Si, Pb, Br, among others), shedding light into their paleoenvironmental significance. To our knowledge, this is the first attempt to use such a wide array of geochemical proxies, providing solid arguments to explore their potential in future works.

7- Conclusions

Dense and complex elemental archives of seventeen bivalve shells belonging to two neighbouring Upper Albian shallow-water sections (western Portugal) were explored using a thorough statistical analysis protocol, comparing mono- and multi-species datasets, as well as shells from different locations.

Several conclusions were extracted from applying the double PCA+ approach:

(i) Syn- to post-depositional processes can easily be identified based on the characteristic elemental associations revealed by PCA results. These include the influence of diagenesis (Fe, Mn and Mg); shell-borings filled by terrigenous materials (persistent coupling of Si, Al, Fe and Mg); bioaccumulation of heavy metals (Pb, Zn) and Br due to stabilization of organic shell components;

(ii) Different elemental patterns may arise, depending on the variability of the sampled materials. For mono-species groups, the tight clustering of less-altered samples provides a very clear decoupling of samples responding to syn and post-depositional processes. This may also be the case for multi-species datasets, but if the original differences in elemental incorporation are significant, several main clusters arise, which should be analyzed separately to disentangle species-specific from depositional effects on trace element content;

(iii) Background elemental signals (calcification mechanism and/or environmental) are typically interrupted by two main types of disruption: one locally affecting only a minor portion of the shell, thus characterized by sharp and very significant changes in elemental composition (e.g., boring); the second affecting a larger portion of the shell, but in a less prominent elemental shift (e.g., recrystallizations);

(iv) Regardless the degree of shell-alteration, our PCA+ approach successfully isolated paleoenvironmental signals. The less-altered portions of the shells provided the establishment of dynamic cut-off values, customized for each set of shells and in overall agreement with elemental data retrieved from the literature. More unconventional elemental data also responded well to the double PCA+ approach, contributing with new clues for unravelling their incorporation mechanisms in ancient shells (Cu, P, S, Cl, K, Br, Zn, Pb).

This research provides new and relevant methodological advances, underlining the need to explore this and other tools that counterbalance the increasing technical ability to obtain dense, but highly intricate sclerochronological datasets and the most efficient way to unveil hidden, but relevant paleoenvironmental information. Expanding the use of the presented double PCA+ approach to other skeletal materials and time slices is thus a promising path towards a deeper understanding of past climatic dynamics, biomineralization processes and shell-archives and diagenetic pathways over time, providing solid arguments to explore their potential in future works.

Acknowledgements

R. Coimbra is supported by Fundação para a Ciência e Tecnologia- FCT, Portugal and the research unit GeoBiotec - UIDB/04035/2020. Collection and preparation of fossil shell material was supported by DFG grant HE4467/6-1 to U. Heimhofer. PC thanks Research Foundation Flanders FWO-Hercules foundation for the acquisition of the µXRF instrument, and VUB Strategic Research. NdW is a Flemish Research Foundation (FWO; 12ZB220N) post-doctoral fellow, and is supported by a MSCA Individual Fellowship (H2020-MSCA-IF-2018; 843011 – UNBIAS).

References

Abdi, H., Williams, L.J., 2010. Principal component analysis. Wiley Interdisciplinary Reviews: Computational Statistics 2, 433-459.

Al-Aasm, I.S. and Veizer, J.J., 1982. Chemical stabilization of low-magnesium calcite: an example of brachiopods. Journal of Sedimentary Petrology, 52, 1101-1109.

Al-Aasm, I.S., Veizer, J., 1986a. Diagenetic stabilization of aragonite and low-Mg calcite, II. Stable isotopes in rudists. Journal of Sedimentary Research 56, 763-770.

Al-Aasm, I.S., Veizer, J., 1986b. Diagenetic stabilization of aragonite and low-Mg calcite, I. Trace elements in rudists. Journal of Sedimentary Research 56, 138-152.

Batenburg, S.J., Reichart, G.-J., Jilbert, T., Janse, M., Wesselingh, F.P., Renema, W., 2011. Interannual climate variability in the Miocene: High resolution trace element and stable isotope ratios in giant clams. Palaeogeography, Palaeoclimatology, Palaeoecology 306, 75-81.

Berthou, P.-Y., 1984. Albian-Turonian stage boundaries and subdivisions in the western Portuguese Basin, with special emphasis on the Cenomanian-Turonian boundary in the ammonite facies and rudist fades. Bulletin of the Geological Society of Denmark 33, 41-45.

Brand, R., 2006. Scallop ecology: distributions and behaviour. *In*: Shumway, S.E., Parsons, G.J. (Eds.), Scallops: Biology, Ecology and Aquaculture. Elsevier B.V, Amsterdam, The Netherlands, 651-744.

Brand, U., Veizer, J., 1980. Chemical diagenesis of a multicomponent carbonate system - 1: Trace elements. Journal of Sedimentary Research 50, 1219-1236.

Brand, U., Veizer, J., 1981. Chemical diagenesis of a multicomponent carbonate system-2: stable isotopes. Journal of Sedimentary Research 51, 987-997.

Cai, T., Wu, H., Qin, J., Qiao, J., Yang, Y., Wu, Y., Qiao, D., Xu, H., Cao, Y., 2019. In vitro evaluation by PCA and AHP of potential antidiabetic properties of lactic acid bacteria isolated from traditional fermented food. LWT 115, 108455.

Carter, J.G., 1990. Skeletal biomineralization: patterns, processes and evolutionary trends. Van Nostrand & Reinhold, New York, 832 pp.

Chan, P., Halfar, J., Williams, B., Hetzinger, S., Steneck, R., Zack, T., Jacob, D.E., 2011. Freshening of the Alaska Coastal Current recorded by coralline algal Ba/Ca ratios. Journal of Geophysical Research: Biogeosciences 116 (G1).

Carré, M., Bentaleb, I., Bruguier, O., Ordinola, E., Barrett, N.T., Fontugne, M., 2006. Calcification rate influence on trace element concentrations in aragonitic bivalve shells: Evidences and mechanisms. Geochimica et Cosmochimica Acta 70, 4906-4920.

Christ, N., Immenhauser, A., Amour, F., Mutti, M., Tomás, S., Agar, S.M., Alway, R., Kabiri, L., 2012. Characterization and interpretation of discontinuity surfaces in a Jurassic ramp setting (High Atlas, Morocco). Sedimentology 59, 249-290.

Chumakov, N.M., Zharkov, M.A., Herman, A.B., Doludenko, M.P., Kalandadze, N.N., Lebedev, E.A., Ponomarenko, A.G., Rautian, A.S., 1995. Climate belts of the mid Cretaceous time. Stratigraphy and Geological Correlations 3, 241-260.

Coimbra, R., Azerêdo, A.C., Cabral, M.C., 2018. Cretaceous coastal lagoon facies: Geochemical insights into multi-stage diagenesis and palaeoclimatic signals. Cretaceous Research 85, 60-77.

Coimbra, R., Horikx, M., Huck, S., Heimhofer, U., Immenhauser, A., Rocha, F., Dinis, J., Duarte, L.V., 2017. Statistical evaluation of elemental concentrations in shallow-marine deposits (Cretaceous, Lusitanian Basin). Marine and Petroleum Geology 86, 1029-1046.

Coimbra, R., Immenhauser, A., Olóriz, F., Rodríguez-Galiano, V., Chica-Olmo, M., 2015. New insights into geochemical behaviour in ancient marine carbonates (Upper Jurassic Ammonitico Rosso): Novel proxies for interpreting sea-level dynamics and palaeoceanography. Sedimentology 62, 266-302.

Cordella, C.B.Y., 2012. PCA: The Basic Building Block of Chemometrics. In: Krull, I. S. (director), Analytical Chemistry, pp. 1-44.

Damas-Mollá, L., Aranburu-Artano, A., García-Garmilla, F., 2006. Resistencia a la alteración diagenética de conchas de Chondrodonta sp. en las calizas rojas del Aptiense-Albiense Inferior de Ereño (Bizkaia). Geogaceta, 40, 195-198.

de Winter, N. J., Goderis, S., Dehairs, F., Jagt, J. W., Fraaije, R. H., Van Malderen, S. J., et al. (2017). Tropical seasonality in the late Campanian (late Cretaceous): Comparison between multiproxy records from three bivalve taxa from Oman. Palaeogeography, Palaeoclimatology, Palaeoecology, 485, 740-760.

de Winter, N. J., Vellekoop, J., Vorsselmans, R., Golreihan, A., Soete, J., Petersen, S. V., et al. (2018). An assessment of latest Cretaceous Pycnodonte vesicularis (Lamarck, 1806) shells as records for palaeoseasonality: a multi-proxy investigation. Climate of the Past, 14(6), 725-749.

Dinis, J. L., Rey, J., De Graciansky, P. C., 2002. The Lusitanian Basin (Portugal) during the late Aptian- Albian: Sequential arrangement, proposal of correlations, evolution. Comptes Rendus Geoscience 334 (10), 757-764.

Dinis, J. L., Trincão, P., 1995. Recognition and stratigraphical significance of the Aptian unconformity in the Lusitanian Basin, Portugal. Cretaceous Research 16 (2-3), 171-186.

Dinis, J.L., Rey, J., Cunha, P.P., Callapez, P., Pena dos Reis, R., 2008. Stratigraphy and allogenic controls of the western Portugal Cretaceous: an updated synthesis. Cretaceous Research 29, 772-780.

Du, Y., Lian, F., Zhu, L., 2011. Biosorption of divalent Pb, Cd and Zn on aragonite and calcite mollusk shells. Environmental Pollution 159, 1763-1768.

Elderfield, H., M. Vautravers, and M. Cooper, 2002. The relationship between shell size and Mg/Ca, Sr/Ca, $\delta^{18}O$, and $\delta^{13}C$ of species of planktonic foraminifera. Geochemistry, Geophysics, Geosystems 3(8), 1-13.

Ferreira, A.G., Machado, A.L.S., Zalmon, I.R., 2004. Temporal and spatial variation on heavy metal concentrations in the bivalve Perna perna (LINNAEUS, 1758) on the northern coast of Rio de Janeiro State, Brazil. Brazilian Archives of Biology and Technology 47, 319-327.

Furuhashi, T., Schwarzinger, C., Miksik, I., Smrz, M., Beran, A., 2009. Molluscan shell evolution with review of shell calcification hypothesis. Comparative Biochemistry and Physiology Part B: Biochemistry and Molecular Biology 154, 351-371.

Gili, E., Götz, S., 2018. Part N, Volume 2, Chapter 26B: Paleoecology of rudists. Treatise Online 103: 1-29.

Gili, E., Masse, J.P., Skelton, P.W., 1995. Rudists as gregarious sediment-dwellers, not reef-builders, on Cretaceous carbonate platforms. Palaeogeography, Palaeoclimatology, Palaeoecology 118, 245-267.

Gillikin, D.P., Lorrain, A., Paulet, Y.-M., André, L., Dehairs, F., 2008. Synchronous barium peaks in high-resolution profiles of calcite and aragonite marine bivalve shells. Geo-Marine Letters 28, 351-358.

Gillikin, D.P., Lorrain, A., Paulet, Y.M., André, L., Dehairs, F., 2008. Synchronous barium peaks in high-resolution profiles of calcite and aragonite marine bivalve shells. Geo- Marine Letters 28 (5-6), 351-358.

Gillikin, D.P., Wanamaker, A.D., Andrus, C.F.T., 2019. Chemical sclerochronology. Chemical Geology 526, 1-6.

Gingerich, P.D., 2006. Environment and evolution through the Paleocene-Eocene thermal maximum. Trends in ecology & evolution 21, 246-253.

Grégoire, C., 1972. Structure of the molluscan shell. In: Florkin, M., Scheer, B.T. (Eds.) Chemical Zoology. Academic Press, New York, Vol. 7, pp. 45-102.

Grice, K., Cao, C., Love, G.D., Böttcher, M.E., Twitchett, R.J., Grosjean, E., Summons, R.E., Turgeon, S.C., Dunning, W., Jin, Y., 2005. Photic zone euxinia during the Permian-Triassic superanoxic event. Science 307, 706-709.

Halfar, J., Zack, T., Kronz, A., Zachos, J.C., 2000. Growth and high-resolution paleoenvironmental signals of rhodoliths (coralline red algae): a new biogenic archive. Journal of Geophysical Research: Oceans 105 (C9), 22107-22116.

Harper et al., 1996. Early Cretaceous cementing pectinid bivalves. Cretaceous Research 17, 135-150.

Hasenboehler, B., 1981. Étude paleobotanique et palynologie de l'Albien et du Cénomanien du "Bassin Occidental Portugais" au sud de l'accident de Nazaré (Portugal). Université Pierre et Marie Curie, Paris, Thése 3éme Cycle. Unpublished PhD thesis, 348 pp.

Heimhofer, U., Hochuli, P. A., Burla, S., Weissert, H., 2007. New records of Early Cretaceous angiosperm pollen from Portuguese coastal deposits: Implications for the timing of the early angiosperm radiation. Review of Palaeobotany and Palynology 144(1), 39-76.

Heuer, A.H., Su, X., Kamat, S., Ballarini, R., Buschow, K.H.J., Cahn, R.W., Flemings, M.C., Ilschner, B., Kramer, E.J., Mahajan, S., Veyssiüre, P., 2001. Shell: Properties. In: Jürgen Buschow, K. H., Cahn, R.W., Flemings, M. C., Ilschner, B., Kramer, E., Mahajan, S., Veyssière, P. (Eds.), Encyclopedia of Materials: Science and Technology. Elsevier, Oxford, pp. 8462-8469.

Higuera, I.R., Garmilla, F.G., Skelton, P.W., 2007. Sclerochronology and diagenesis of Late Cretaceous radiolitids (Bivalvia, Hippuritoidea), Spain. In: Scott, R.W. (Ed.), Cretaceous rudists and carbonate platforms: environmental feedback. SEPM Special Publication, 87, pp. 115-139.

Horikx, M., Heimhofer, U., Dinis, J., Huck, S., 2014. Integrated stratigraphy of shallow marine Albian strata from the southern Lusitanian Basin of Portugal. Newsletters on Stratigraphy 47, 85-106.

Horikx, M., Hochuli, P.A., Feist-Burkhardt, S., Heimhofer, U., 2016. Albian angiosperm pollen from shallow marine strata in the Lusitanian Basin, Portugal. Review of Palaeobotany and Palynology 228, 67-92.

Huyghe, D., de Rafelis, M., Ropert, M., Mouchi, V., Emmanuel, L., Renard, M., Lartaud, F., 2009. New insights into oyster high-resolution hinge growth patterns. Marine Biology 166, 48.

Immenhauser, A., Schöne, B.R., Hoffmann, R., Niedermayr, A., 2018. Mollusc and brachiopod skeletal hard parts: Intricate archives of their marine environment. Sedimentology 63, 1-59.

Jacob, D.E., Soldati, A.L., Wirth, R., Huth, J., Wehrmeister, U., Hofmeister, W., 2008. Nanostructure, composition and mechanisms of bivalve shell growth. Geochimica et Cosmochimica Acta 72, 5401-5415.

Jones, D.S., 1983. Sclerochronology: Reading the Record of the Molluscan Shell: Annual growth increments in the shells of bivalve molluscs record marine climatic changes and reveal surprising longevity. American Scientist 71, 384-391.

Jones, K., Bronson, S., Brink, P., Gordon, C., Mosher-Smith, K., Brown, M., Chaudhry, S., Rizzo, A., Sigismondi, R., Whitehurst, M., Lukaszewski, A., Kranz, D., Bland, K., Gordan, D., Lobel, J., Sullivan, J., Metzger, M., Shea, C., Harris, C., Kambhampati, M., 2009. Bivalve Characterization Using Synchrotron Micro X-Ray Fluorescence. Acta Physica Polonica A 115.

Kullberg, J. C., Rocha, R. B., Soares, A. F., Rey, J., Terrinha, P., Azerêdo, A. C., Callapez, P., Duarte, L. V., Kullberg, M. C., Martins, L., Miranda, J. R., Alves, C., Mata, J., Madeira, J., Mateus, O., Moreira, M., Nogueira, C.R., 2013. A Bacia Lusitaniana: Estratigrafia, Paleogeografia e Tectónica. In Geologia de Portugal (eds. R. Dias, A. Araújo, P. Terrinha and J-C. Kullberg). Volume 2, Escolar Editora, Lisbon, Portugal, pp. 195-347.

LNEG-LGM, 2010. Carta Geológica de Portugal à escala 1:1000000, edição de 2010. Laboratório Nacional de Energia e Geologia, Lisbon, Portugal.

Lorens, R. B., 1981. Sr, Cd, Mn, and Co distribution coefficients in calcite as a function of calcite precipitation rate. Geochimica et Cosmochimica Acta, 45, 553-561.

Markulin, K.i., Peharda, M., Mertz-Kraus, R., Schöne, B.R., Uvanovič, H., Kovač, Ž., Janeković, I., 2019. Trace and minor element records in aragonitic bivalve shells as environmental proxies. Chemical Geology 507, 120-133.

Medus, J., 1982. Palynofloristic correlations of two Albian sections of Portugal. Cuadernos Geología Ibérica 8, 781-809.

Nedoncelle, K., Lartaud, F., de Rafelis, M., Boulila, S., Le Bris, N., 2013. A new method for high-resolution bivalve growth rate studies in hydrothermal environments. Marine Biology 160, 1427-1439.

Nürnberg, D., Bijma, J., Hemleben, C., 1996. Assessing the reliability of magnesium in foraminiferal calcite as a proxy for water mass temperatures. Geochimica et Cosmochimica Acta 60, 803-814.

Philip, J., 1972. Paléoécologie des formations à rudistes du Crétacé supérieur - l'exemple du sud-est de la France. Palaeogeography, Palaeoclimatology, Palaeoecology 12, 205-222.

Pokroy, B., Fitch, A., Zolotoyabko, E., 2006. The Microstructure of Biogenic Calcite: A View by High-Resolution Synchrotron Powder Diffraction. Advanced Materials 18, 2363-2368.

Pons, J.-M., Vicens, E. , 2008. The structure of the outer shell layer in radiolitid rudists, a morphoconstructional approach. Lethaia 41, 219-234.

Rauch, M., 2005. Geochemie von Rudistenschalen - Beiträge zur Meerwasserchemie (Sr/Ca, Mg/Ca, $\delta^{13}C$) und Paläoklima der Kreide. PhD thesis, 198 pp., Ruhr-University Bochum, Bochum, Germany.

Rey, J., 1992. Les unités lithostratigraphiques du Crétacé inférieur de la région de Lisbonne. Comunicações dos Serviços Geológicos de Portugal 78, 103-124.

Richardson, C.A., Peharda, M., Kennedy, H., Kennedy, P., Onofri, V., 2004. Age, growth rate and season of recruitment of Pinna nobilis (L) in the Croatian Adriatic determined from Mg: Ca and Sr: Ca shell profiles. Journal of Experimental Marine Biology and Ecology 299, 1-16.

Rickaby, R. E. M. , Schrag, D. P. , Zondervan, I. and Riebesell, U. (2002): Growth-rate dependence of Sr incorporation during calcification of Emiliania huxleyi, Global Biogeochemical Cycles, 16 (1), 1-8.

Rimstidt, J.D., Balog, A., Webb, J., 1998. Distribution of trace elements between carbonate minerals and aqueous solutions. Geochimica et Cosmochimica Acta 62, 1851-1863.

Ross, D.J., Skelton, P.W., 1993) Rudist formations of the Cretaceous: A palaeoecological, sedimentological and stratigraphical review. Sedimentology Review 1, 73-91.

Schöne, B. R., Zhang, Z., Radermacher, P., Thébault, J., Jacob, D. E., Nunn, E. V., & Maurer, A.-F. (2011). Sr/Ca and Mg/Ca ratios of ontogenetically old, long-lived bivalve shells (Arctica islandica) and their function as paleotemperature proxies. Palaeogeography, Palaeoclimatology, Palaeoecology, 302(1-2), 52-64.

Schöne, B.R., Fiebig, J., Pfeiffer, M., Gleβ, R., Hickson, J., Johnson, A.L., Dreyer, W., Oschmann, W., 2005. Climate records from a bivalved Methuselah (Arctica islandica, Mollusca; Iceland). Palaeogeography, Palaeoclimatology, Palaeoecology 228, 130-148.

Schöne, B.R., Houk, S.D., Castro, A.D.F., Fiebig, J., Oschmann, W., Kröncke, I., Dreyer, W., Gosselck, F., 2005. Daily growth rates in shells of Arctica islandica: assessing sub-seasonal environmental controls on a long-lived bivalve mollusk. Palaios 20, 78-92.

Serb, J.M., 2006. Reconciling morphological and molecular approaches in developing a Phylogeny for the Pectinidae (Mollusca: Bivalvia). In: Shumway, S.E., Parsons, G.J. (Eds.), Scallops: Biology, Ecology and Aquaculture. Elsevier B.V, Amsterdam, The Netherlands, 1-29.

Skelton, P.W., 1978. The evolution of functional design in rudists (Hippuritacea) and its taxonomic implications. Royal Society of London, Philosophical Transactions 284, 305-318.

Skelton, P.W., 2003. The Cretaceous World. The Open University and Cambridge University Press. Cambridge, UK. 360 pp.

Skelton, P.W., 2018. Part N, Volume 1, Chapter 26A: Introduction to the Hippuritida (rudists): Shell structure, anatomy, and evolution. Treatise Online 104: 1-37.

Skelton, P.W., Smith, A.B., 2000. A preliminary phylogeny for rudist bivalves: Sifting clades from grades. *In*: Harper, E.M, Taylor, J.D., Crame, J.A. (Eds.): The Evolutionary Biology of the Bivalvia. Geological Society, London, Special Publications 177, 97-127.

Stampfli, G.M., Borel, G.D., 2002. A plate tectonic model for the Paleozoic and Mesozoic constrained by dynamic plate boundaries and restored synthetic oceanic isochrons. Earth and Planetary Science Letters 196, 17-33.

Stanley, S.M., 1970. Relation of shell form to life habits of the Bivalvia (Mollusca). Geological Society of America Memoires 125, 1-296.

Steuber, T., 1996. Stable isotope sclerochronology of rudist bivalves: Growth rates and Late Cretaceous seasonality. Geology, 24, 315-318.

Steuber, T., 1999. Isotopic and chemical intra-shell variations in low-Mg calcite of rudist bivalves (Mollusca-Hippuritacea): disequilibrium fractionations and late Cretaceous seasonality. International Journal of Earth Sciences 88, 551-570.

Steuber, T., 2000. Skeletal growth rates of Upper Cretaceous rudist bivalves: implications for carbonate production and organism-environment feedbacks. In: INSALCO, E. et al. (eds.): Carbonate Platform Systems: Components and Interactions. Geol. Soc. London, Spec. Publ., 178, 21-32.

Steuber, T., Rauch, M., Masse, J.-P., Graaf, J., Malkoč, M., 2005. Low-latitude seasonality of Cretaceous temperatures in warm and cold episodes. Nature 437, 1341-1344.

Stoll, H.M., Klaas, C.M., Probert, I., Ruiz Encinar, J., Garcia Alonso, J.I., 2002. Calcification rate and temperature effects on Sr partitioning in coccoliths of multiple species of coccolithophorids in culture. Global and Planetary Change 34, 153-171.

Stoll, H.M., Schrag, D.P., 2000. Coccolith Sr/Ca as a new indicator of coccolithophorid calcification and growth rate. Geochemistry, Geophysics, Geosystems (1), 1006.

Surge, D., Lohmann, K. C., & Dettman, D. L. (2001). Controls on isotopic chemistry of the American oyster, Crassostrea virginica: implications for growth patterns. Palaeogeography, Palaeoclimatology, Palaeoecology, 172(3), 283-296.

Swart, P.K., 2015. The geochemistry of carbonate diagenesis: the past, present and future. Sedimentology 62, 123-e1304.

Tesoriero, A. J., and J. F. Pankow, 1996. Solid solution partitioning of Sr^{2+}, Ba^{2+} and Cd^{2+} to calcite. Geochimica et Cosmochimica Acta, 60, 1053-1063, 1.

Tibljaš, D., Moro, A., Ostrež, Ž., 2004. Mineral and Chemical Composition of Rudist Valves from Upper Cretaceous Limestones of Southern Istria, Croatia. Geologia Croatica, 57 (1), 73-79.

Ullmann, C.V., Gale, A.S., Huggett, J., Wray, D., Frei, R., Korte, C., Broom-Fendley, S., Littler, K., Hesselbo, S.P., 2018. The geochemistry of modern calcareous barnacle shells and applications for palaeoenvironmental studies. Geochimica et Cosmochimica Acta 243, 149-168.

Ullmann, C.V., Wiechert, U., Korte, C., 2010. Oxygen isotope fluctuations in a modern North Sea oyster (Crassostrea gigas) compared with annual variations in seawater temperature: Implications for palaeoclimate studies. Chemical Geology 277, 160-166.

VanPlantinga, A.A., Grossman, E.L., 2019. Trace elements in mussel shells from the Brazos River, Texas: environmental and biological control. Biogeosciences Discussions 2019, 1-27.

Veizer, J., 1983. Chemical analysis of carbonates: theory and application of trace element technique. In: Arthur, M.A., Anderson, T.F., Kaplan, I.R., Veizer, J. (Eds.), Stable Isotopes in Sedimentary Geology. SEPM Short Course No.10, pp. 1-100.

Yao, F., Coquery, J., Lê-Cao, K.-A., 2012. Independent Principal Component Analysis for biologically meaningful dimension reduction of large biological data sets. BMC bioinformatics 13, 24-24.

Zachos, J., Pagani, M., Sloan, L., Thomas, E., Billups, K., 2001. Trends, rhythms, and aberrations in global climate 65 Ma to present. Science 292, 686-693.

Zamarreño et al., 1996. The shell microstructure, mineralogy and isotopic composition of Amussiopecten baranensis (Pectinidae, Bivalvia) from the Miocene of Spain: A valuable paleoenvironmental tool Geobios 29, 707-724.

Figure captions

Fig. 1. Geographical setting of the studied locations. A) Map of Iberia showing the location of the western Portuguese coast. B) Regional distribution of Cretaceous outcrops (adapted from LNEG-LGM, 2010), along with delimitation of the Lusitanian Basin (after Kullberg et al., 2013). C) Location of study sites at São Julião and Praia das Maçãs (indicated by stars), south of Ericeira (Portugal).

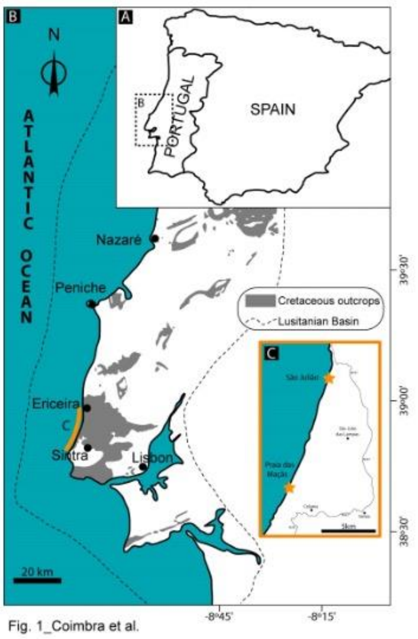

Fig. 1_Coimbra et al.

Fig. 2. Field photographs and particular aspects of sampled beds and shells. A and B) Aerial photographs of Praia das Maçãs and near São Julião (extracted from http://portugalfotografiaaerea.blogspot.com/); C) Field aspect of one specific sampled bed; D) Field aspect of the pectinid bearing bed at Praia das Maçãs (PM4); E) Field

aspect of a requiniid-rich horizon at Praia das Maçãs (PM12); F) Detail of an *Apricardia carentonensis* shell from the São Julião section.

Fig. 2_Coimbra et al.

Fig. 3. Stratigraphic context, selected specimens and comparison scheme. A) Synthetic lithological log of São Julião and Praia das Maçãs showing height (in meters), stratigraphy, C-isotope values as complementary lateral correlation tool and the main sedimentological features (see Horikx et al., 2014 and Coimbra et al., 2017 for more detailed explanations). B) List of selected specimens and scheme illustrating the logic of comparison followed during this work (see text for further details and Fig. A1 in Appendix for photographs of all used specimens). Numeral tags (in blue) link each shell (or group of shells) specimen to their stratigraphic position, used throughout this contribution.

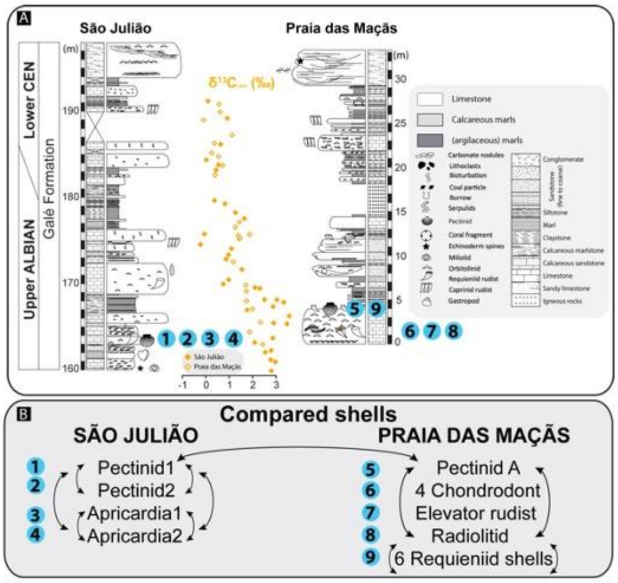

Fig. 3_Coimbra et al.

Fig. 4. Shell structure and preliminary assessment of shell-preservation state. A to D) Example from Praia das Maçãs, including microscope detail of small borings and small cemented (sub-vertical) veinlet and elemental mapping of Mn and Sr, as well as the chosen transect for further geochemical line scanning. E to H) example from São Julião, with microscope detail of small borings and fractures affecting the shell and elemental mapping of Fe and and Mn, as well as the selected transect for further line scanning (red line). Shell length ca. 8 cm in both cases, numeral tags (in blue) are according to Figure 3 and Fig. A1 as Appendix).

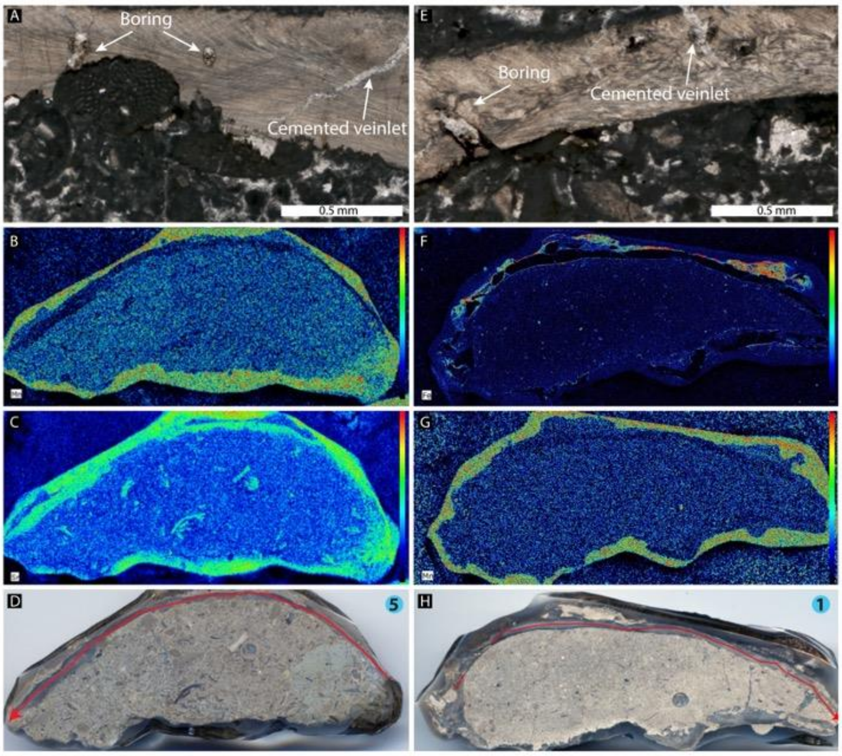

Fig. 4_Coimbra et al.

Fig. 5. Selected raw elemental data (Mn, Fe, Sr, Mg) for two pectinid specimens collected at different locations (Praia das Maçãs and São Julião) illustrating the need of an efficient data treatment approach. Note the high complexity of each elemental record, differences in absolute value and fluctuations along shell-length, as well as the difficulties on comparing the records of both shells. Numeral tags (in blue) are according to Figure 3 and Fig. A1 as Appendix.

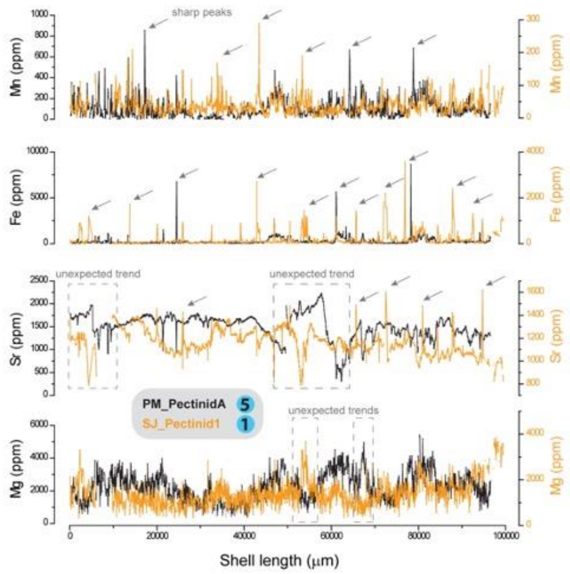

Fig. 5_Coimbra et al.

Fig. 6. Principal component analysis results (scores and loadings), combined with density analysis (see Appendix for further details) for the specimens collected at Praia das Maçãs. Sample distribution by shell is also represented by using coloured dots, corresponding to the contribution of each shell to the cloud of data generated by the PCA procedure (in white dots). This representation is proportional to the main PCA plot, respecting the position of each sample along the PCA space. A) mono-specific analysis including six requiniid shells; B) multi-species analysis including seven different shells belonging to four species. Note tight clustering of a significant percentage of the samples delimiting a range of elemental thresholds, as well as similar elemental trend of deviation from the main cluster (see text for detailed explanation). Numeral tags (in blue) are according to Figure 3 and Fig. A1 as Appendix.

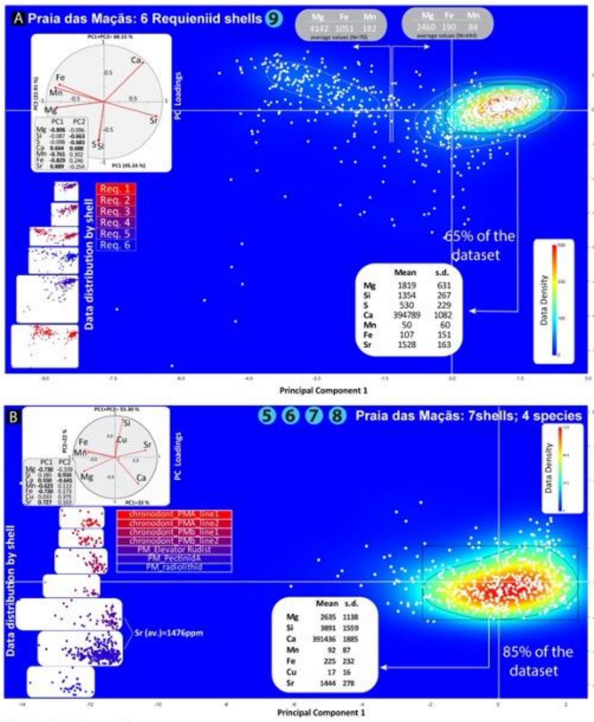

Fig. 6_Coimbra et al.

Fig. 7. Principal component analysis results (PCA scores and loadings), combined with density analysis (double PCA+; see Appendix for further details) for the specimens collected at São Julião. Sample distribution by shell is also represented by using coloured dots, corresponding to the contribution of each shell to the cloud of data generated by the PCA procedure (in white dots). This representation is proportional to the main PCA plot, respecting the position of each sample along the PCA space. A) multi-species analysis including four different shells belonging to two species; B and C) mono-specific analysis of samples included in A), separated by species (*Apricardia* and pectinid, respectively). Note persistent elemental trends when considering different species (see text for detailed explanation). Numeral tags (in blue) are according to Figure 3 and Fig. A1 as Appendix.

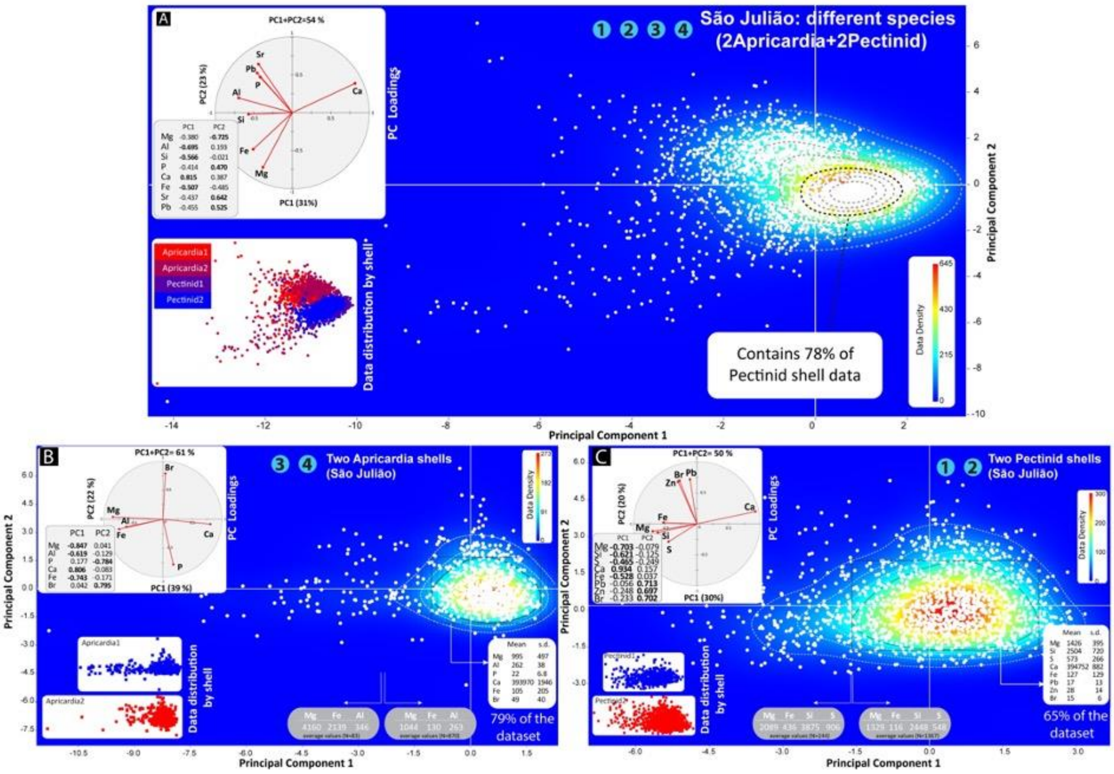

Fig. 7_Coimbra et al.

Fig. 8. Principal component analysis results (PCA scores and loadings), combined with density analysis (double PCA+; see Appendix for further details) for pectinid shells collected at São Julião and Praia das Maçãs (mono-specific analysis). Sample distribution by shell is also represented. Note a tighter clustering of samples belonging to the pectinid shell collected at São Julião (see text for further explanations). Numeral tags (in blue) are according to Figure 3 and Fig. A1 as Appendix.

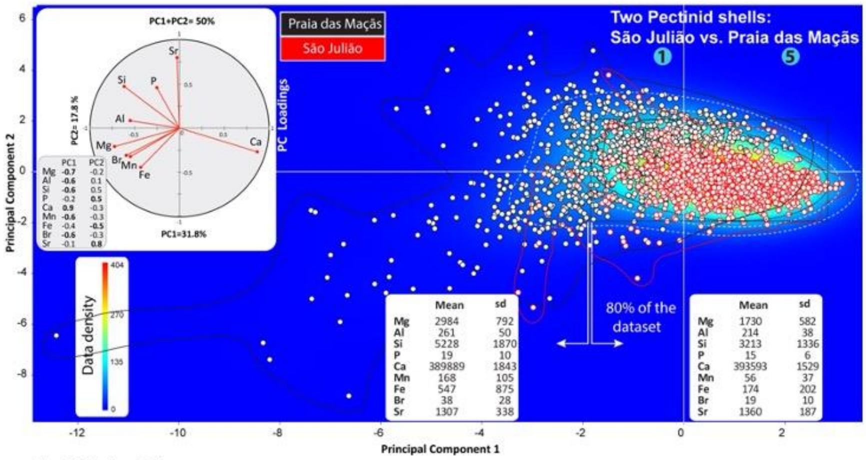

Fig. 8_Coimbra et al.

Fig. 9. Representative scheme of main elemental trends as depicted by double PCA+ approach (see also Fig. A4). A and B) Summary of the persistent elemental trends and associations identified along the tested shells, with their respective process (diagenesis, boring, a combined effect of both and bioaccumulation); C to E) Example of sample distribution across the PCA space in response to the identified processes. Sample distribution will depend on which processes are involved (single or multiple) and on the variability of the biogenic record (mono vs. multi-species analysis).

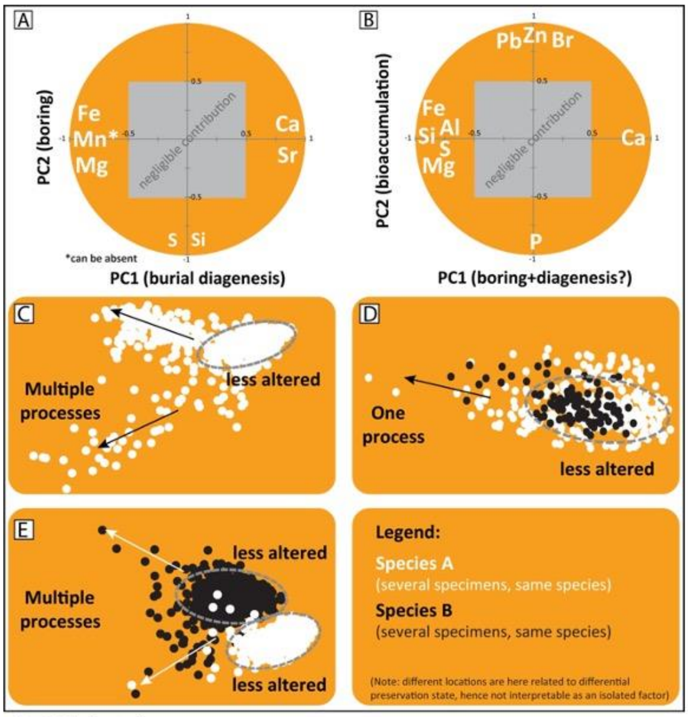

Fig. 9_Coimbra et al.

Fig. 10. Schematic workflow for improving the detection of shell-alteration. A) Possible disruptions of background signal by significantly altered portions and/or cracks; B) fast detection of altered samples allows their elimination from further analysis, in order to obtain a cleaner and relevant paleoenvironmental signal; C) Isolating the clean background record allows the identification of intra-shell fluctuations, attributable to seasonal climate in ancient times. Numeral tags (in blue) are according to Figure 3 and Fig. A1 as Appendix.

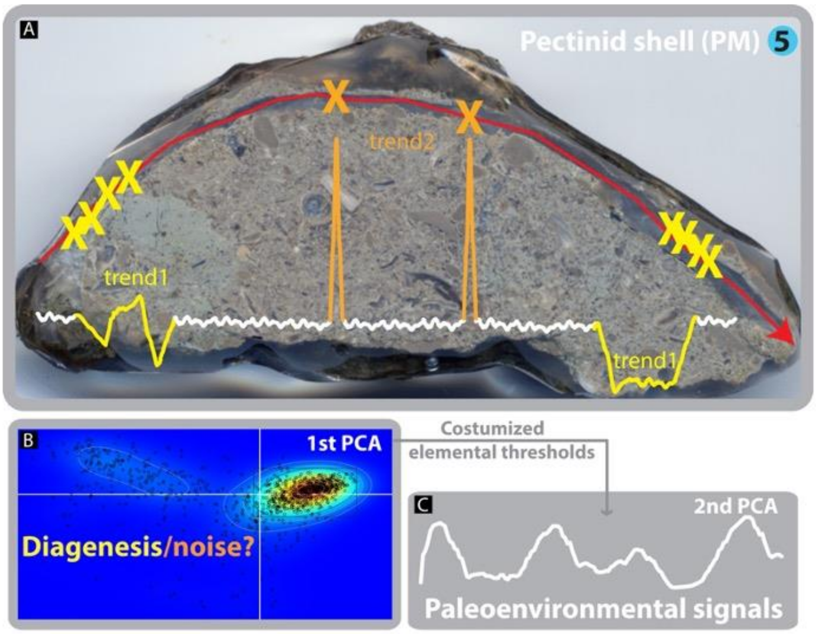

Fig. 10_Coimbra et al.

Fig. 11. Comparison between unprocessed elemental data and the resulting information after the Double PCA+ approach. A) Sr values for the set of 6 requiniid shells (tag numeral as in Figs. 3 and A1). White shaded area delimits the range of best-preserved Sr values, when Double PCA+ is computed for this specific group of shells (see statistic results in Fig. 6). B) Best-preserved Sr values for all requiniid shells, after excluding 20% of the altered data by the Double PCA+ method (see text for details). The clean dataset of each shell now delineates discernible cyclic variations in Sr abundance. Note that the obtained elemental threshold values are customized for this set of mono-speficic shells (see Fig. 12 and Table 1 for obtained values of other sets of shells).

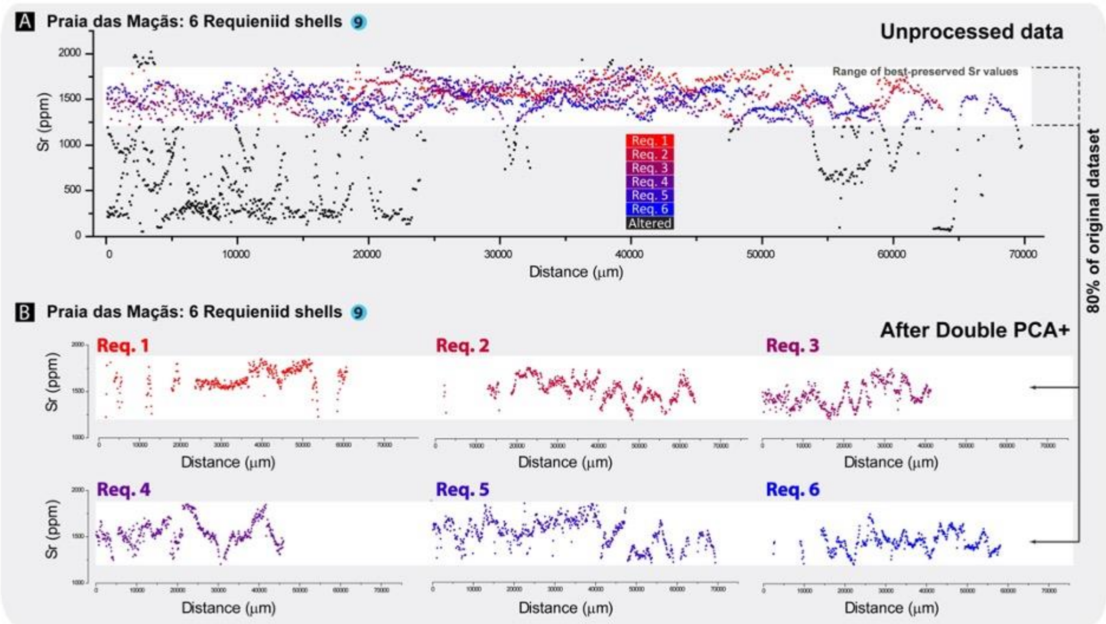

Fig. 11_Coimbra et al.

Fig. 12. Dynamic elemental threshold values obtained by the application of the double PCA+ screening method (see Appendix for details) and data retrieved from available literature. Note overall agreement with published cut-off elemental values, as well and the establishment of new threshold for more unconventional elements (Cu, Zn, Pb, Cu). Numeral tags (in blue) are according to Figure 3 and Fig. A1 as Appendix.

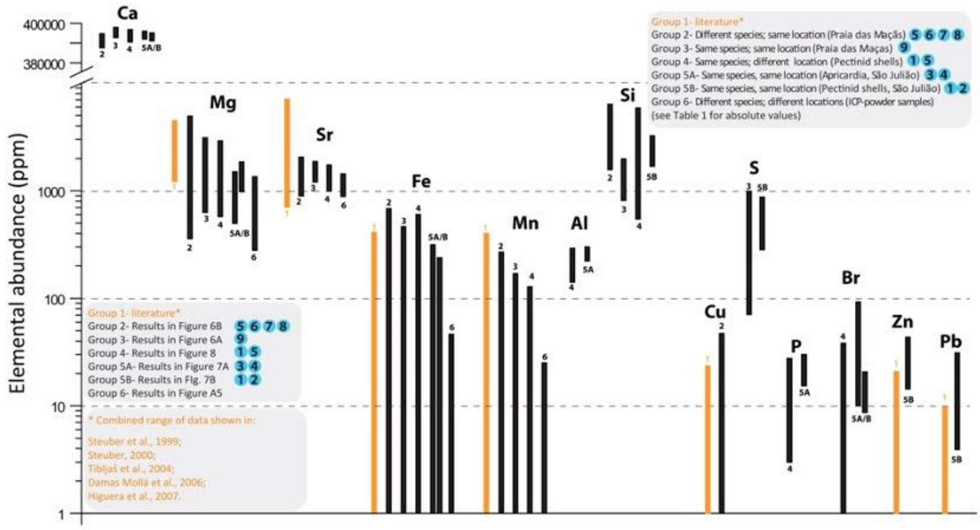

Fig. 12_Coimbra et al.

Table 1. Dynamic elemental threshold values obtained by the application of the double PCA+ screening method (see Appendix for details) and threshold values extracted from literature. Groups 1 to 6 refer to used literature and tested shell combinations (same as in Figure 11). Min=minimum; max=maximum. Numeral tags (in blue) are according to Figure 3 and Fig. A1 as Appendix.

Appendix

1- Materials and methods

Among the richness of shells remains, several specimens were chosen based on their overall preservation state (Fig. A1).

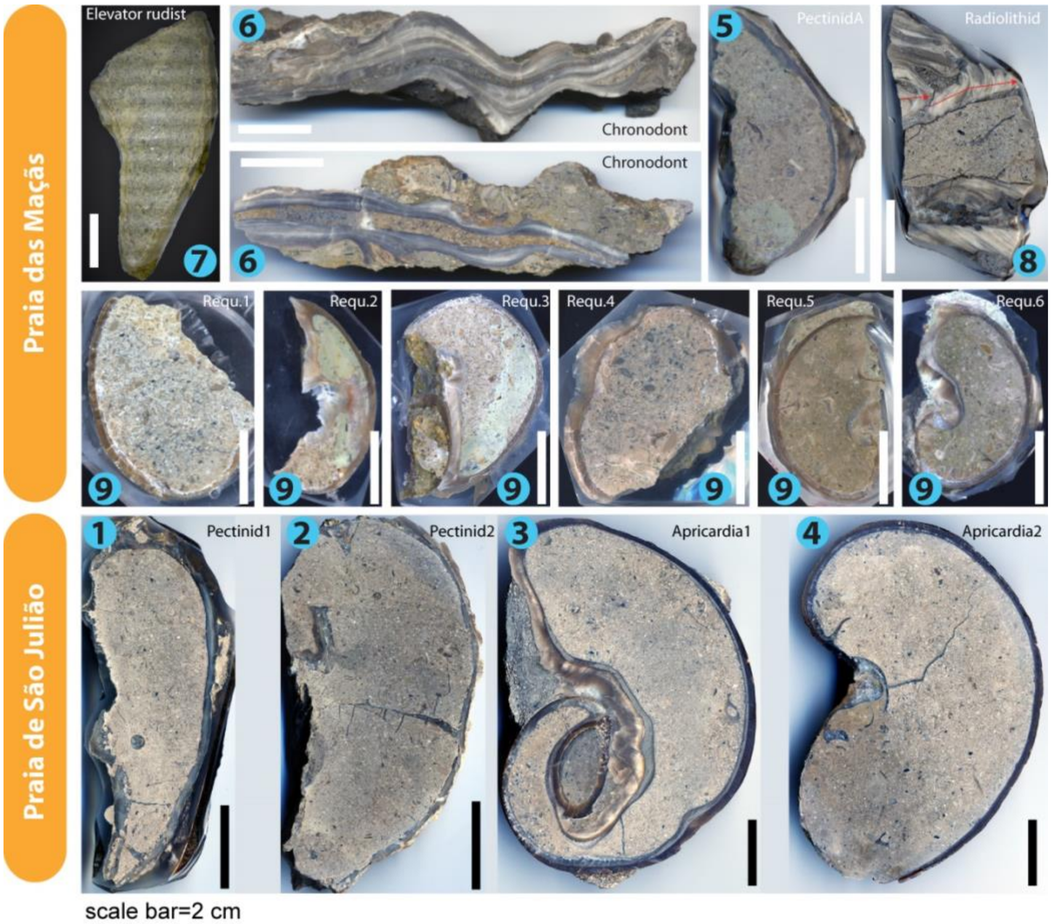

Fig. A1. Sampled shells from both locations. Note the exceptional record of whole shells, whenever possible. Numeral tags (in blue) as in Figure 3.

The vast amount of geochemical variables and resulting datapoints per analysed shell motivated the search for a statistical approach allowing a fast and easy way to perceive otherwise overwhelming information. The detailed step-by-step procedure is given below; the time involved in performing these steps is relatively short, well under 30 minutes.

Because not all the measured proxies resulted in a continuous record though the selected transects, the original dataset presents blanks (i.e., empty cells; See Data Appendix). For each measured transect, only the records with more than 75% of the complete dataset were considered for this contribution ("Count" function on Excel®). This implies that geochemical variables with a high number of blanks are discarded from further computations, maximizing the significance of applied statistical methods. For the surviving variables, missing data was not accepted because this means that not all measured variables have correspondence; hence data rows with blank cells (no data) were discarded (command “Select Blanks” followed by “Delete entire row”). In this way, every measured point has a corresponding value for the most significant variables, and this pre-treatment is performed for each set of samples chosen for comparison. The statistical workflow included a double PCA—double Principal Component Analysis (see also Coimbra et al., 2017 for further details), with intermediate steps assisted by density analysis (Fig. A2).

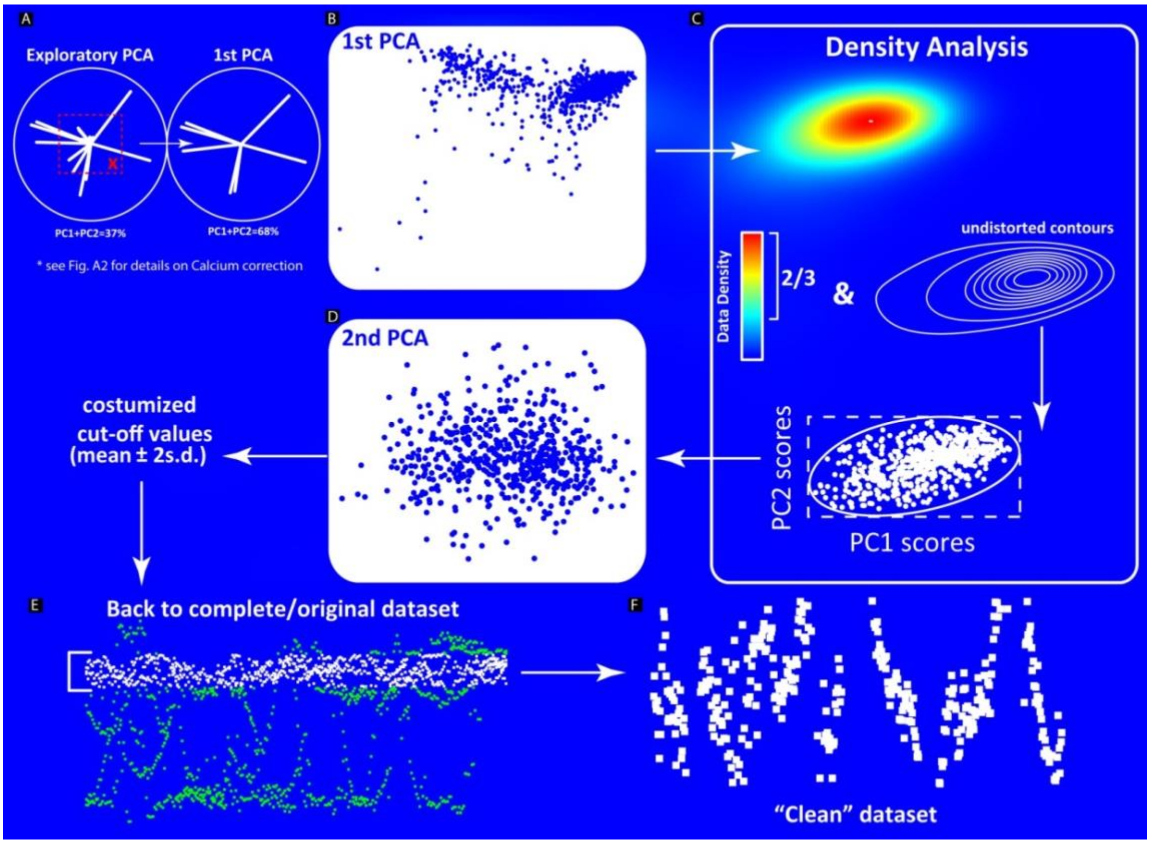

Fig. A2. Statistical workflow leading to a clean elemental dataset. A) Exploratory PCA; B) First PCA; C) Density analysis as an automated delimitation of the main cluster; D) Second PCA. Note the lack of samples deviating from the main cluster, later used to establish the customized cut-off values; E and F) Original dataset with altered samples identified and resulting “clean” dataset, revealing previously masked fluctuations. See text for detailed description and main text for further examples.

Prior to performing the first PCA analysis, an exploratory PCA was performed in order to detect the most significant (loadings <-0.5 and >0.5) geochemical variables for each considered dataset (Fig. A2A). The double PCA was then carried out exclusively for the variables showing higher degree of affinity. It consisted of repeating the PCA procedure in two steps: first with the full dataset, evidencing clear trends on data distribution (Fig. A2B); and secondly by using only the samples that could plot tightly in the first attempt (Fig. A2D). An intermediate step was added in order to assist the selection of the clusters of interest by analysing their distribution through the PCA space: density analysis (Fig. A2C). At this stage, the aim is to automate the process of isolating the samples showing tighter cluster. For this purpose, it is considered that samples plotting within 2/3 of the maximum sample-density and also inside undistorted contour lines to be an optimal choice. The PC scores delimiting this area can then be used to sort and filter the data on the spreadsheet.

The second PCA can now exclusively be performed to samples showing no specific geochemical trend, i.e., the effects of early to late processes strongly affecting the original (paleoenvironmental?) geochemical record are in this way isolated. This situation is evidenced by an evenly spreading cloud of datapoints along the PCA space (Fig. A2D). This set of samples will allow establishing the customized cut-off values for the shell-transect or transects under scope, meaning that these elemental thresholds are not a generalization; they are rather originated from and for this specific dataset. After completing the mentioned steps (Fig. A2A to D), it is possible to go back to the complete original dataset and delimit the range of best-preserved samples (Fig. A2E, F). Because both altered and unaltered samples are relevant for paleoenvironmental and diagenetic interpretations, care was taken to ensure that both cases can easily be accessed at this last step of the procedure.

Elemental abundances may be influenced in a variable degree by the concentration of calcium, the most abundant element in carbonate calcium materials. Such effect may depend on a relative purity of these carbonates or even on the methodological limitations (see Christ et al., 2012 and Coimbra et al., 2015). In order to test this influence on the application of the described procedure, both raw elemental data and calcium-corrected elemental data (element/Ca) were compared for the case of different species collected from one location (Fig. A3).

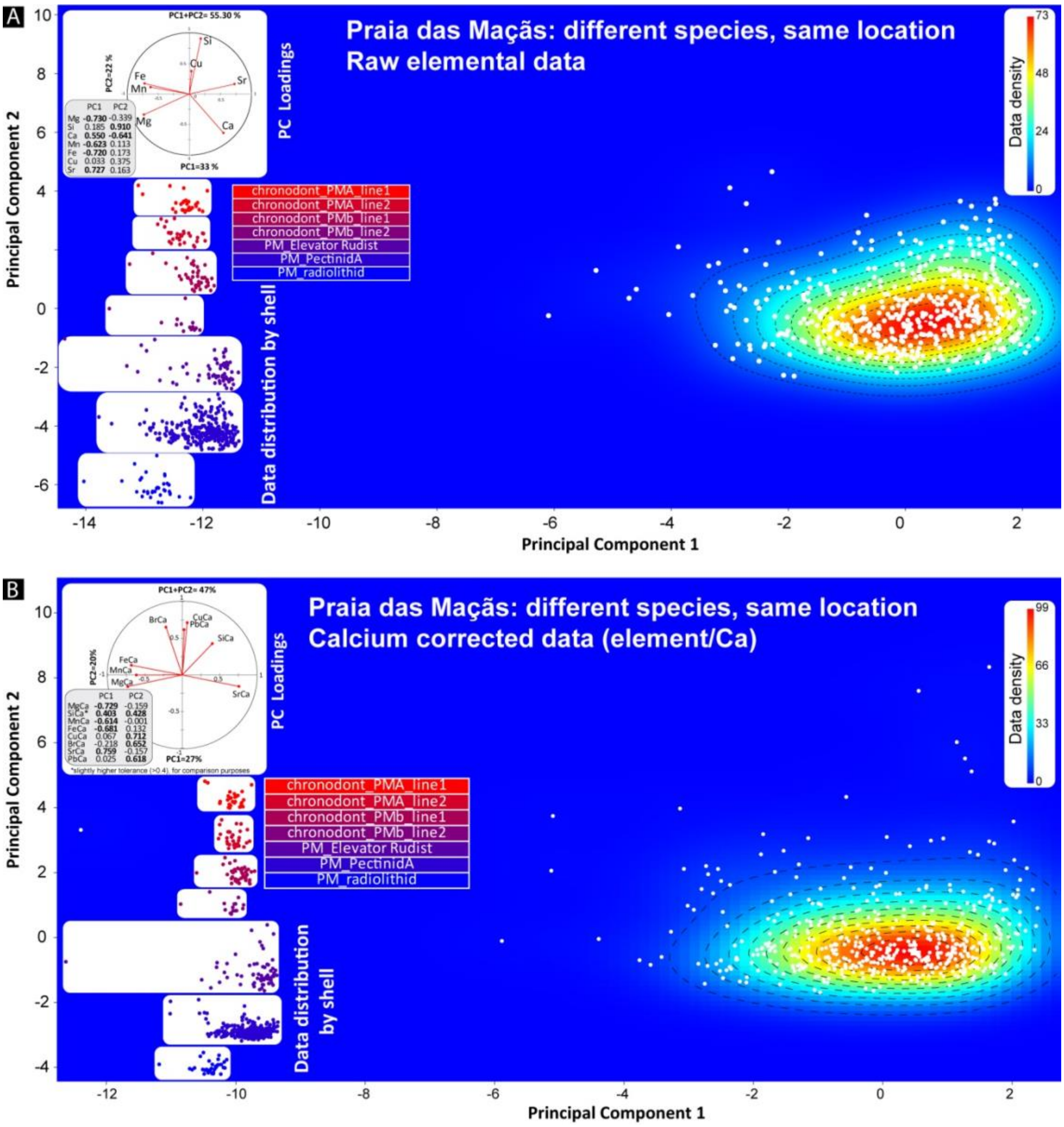

Fig. A3- Example of tested calcium normalization compared to using raw elemental data (Praia das Maçãs, multi-species analysis). Principal component analysis results (PCA scores and loadings), combined with density analysis. Sample distribution by shell is also represented by using coloured dots (red to blue), corresponding to the contribution of each shell to the cloud of data generated by the PCA procedure (in white dots). This representation is proportional to the main PCA plot, respecting the position of each sample along the PCA space.

The most significant variables of PC1 remained exactly the same; PC2 also responded similarly, only adding two minor elements. When considered as a whole, the seven shells do not show major differences, as well as when compared individually: each transect showed a similar sample distribution regardless the applied correction to the elemental data. Obtained differences are therefore only minor, therefore not posing a limitation to the use of raw elemental abundance. This choice is here preferred due to the possibility of comparison with published literature.

Along the same line of reasoning, and because calcium fluctuations could be of relevance regarding the interpretation of carbonate-bound elements, PCA analysis on raw elemental data of all shells retrieved at both locations was compared including Ca, excluding Ca and also by normalizing by Ca abundance (Fig. A4). The lack of major differences in obtained PCA loadings provided further evidence supporting the use of raw elemental data. This stability of the dataset regarding calcium corrections lies on the fact that despite minor fluctuations of this proxy, it remains rather constant in all tested shells, with a standard deviation <1% (mean=393296; sd=2778). This fact is a result of preliminary tests on these materials before performing µXRF scans, ensuring the suitability of the selected shells.

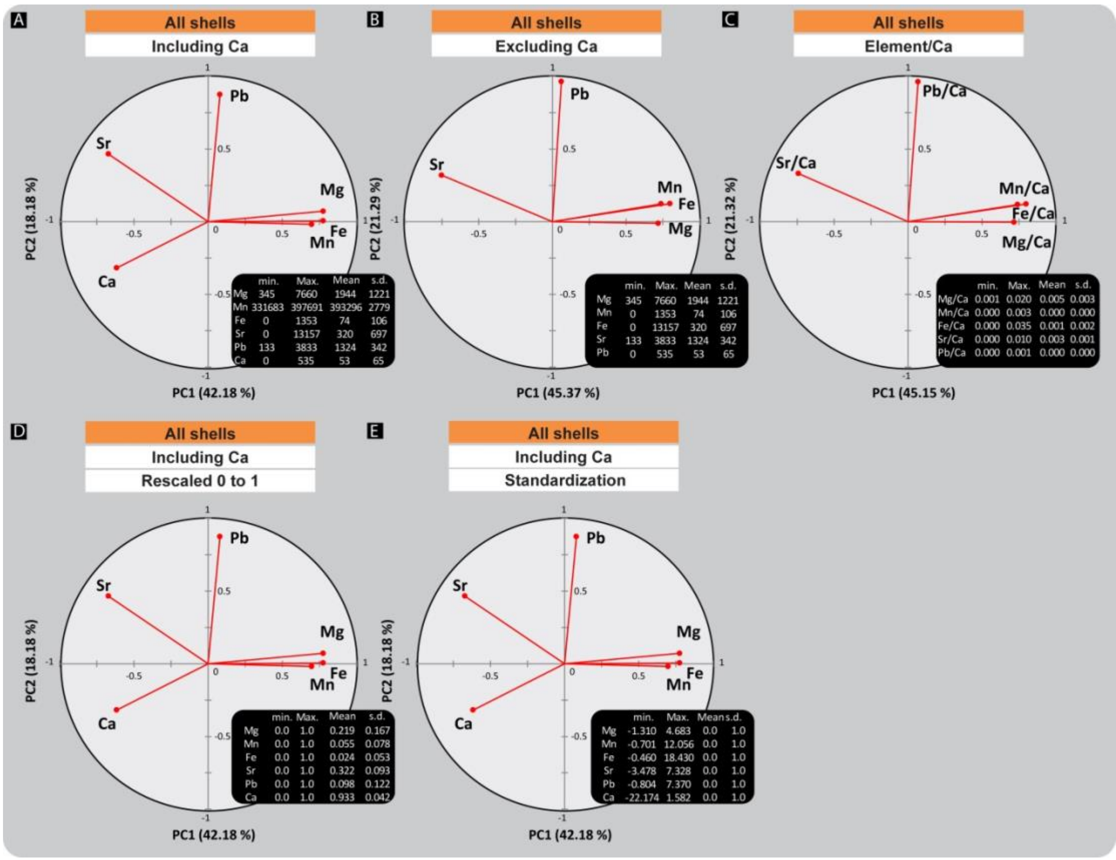

Fig. A4- Principal Component Analysis loadings and respective descriptive statistics (minimum, maximum, mean and standard deviation) computed as preliminary data-treatment tests, performed to elemental data of all shells addressed in this contribution. A) All variables resulting from the pre-treatment described in Materials and Methods (above); B) Excluding Calcium from PCA; C) Normalizing by Calcium; D) Rescaling elemental data from 0 to 1; E) Standardization. Note the persistent trend in elemental associations and lack of relevant differences in all tested possibilities.

Further validation for the applied approach comes from the use of double PCA to a control dataset (Fig. A5) consisting of a large dataset (N=3372 datapoints; in Rauch, 2005) of conventional ICP-AES (inductively coupled plasma - atomic emission spectrometry) elemental data. Elemental data (Mg, Sr, Fe, Mn) and stable isotopes ($\delta^{13}C$, $\delta^{18}O$) from Barremian to Maastrichtian rudist bivalves were here used, belonging to 14 different specimens from 7 locations across Croatia, Spain and France. Although the discussion of this case study falls out of the scope of this contribution, it is noteworthy that most analysed shells cluster tightly along the PCA space (Fig. A5).

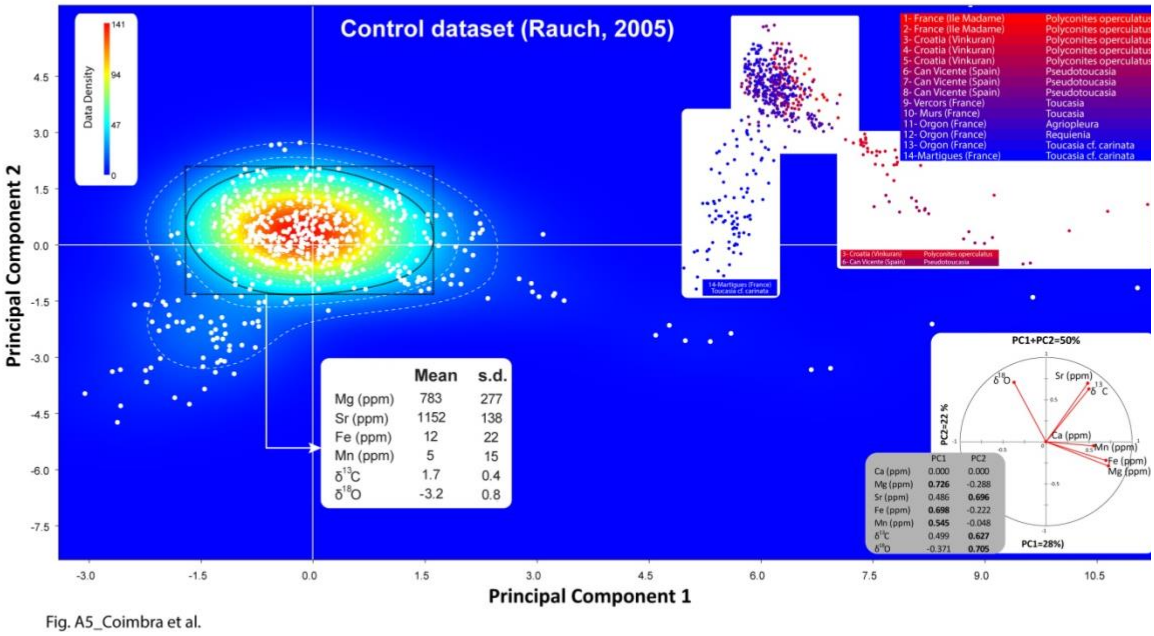

Fig. A5- Principal component analysis results (PCA scores and loadings), combined with density analysis for the control dataset (extracted from Rauch, 2005), consisting on elemental data obtained by ICP-AES (see text). Sample distribution by shell is also represented by using coloured dots, corresponding to the contribution of each shell to the cloud of data generated by the PCA procedure (in white dots). This representation is proportional to the main PCA plot, respecting the position of each sample along the PCA space.

Only three specimens show a clear trend towards differentiated areas of this representation (shells 3, 6 and 14). Accordingly, shells 3 and 6 denote higher Fe, Mn and Mg, accompanied by lowered O-isotope values, a trend attributable to the diagenetic response of these proxies under burial conditions (see main text for further discussion on diagenetic elemental pathways). A different case applies to shell 14, showing depleted Sr and C-isotope values when compared to the main cluster (Fig. A5). Such evidence suggests the influence of meteoric waters during the diagenetic evolution of this shell. These three specimens are therefore altered by an array of diagenetic processes, bearing limited interest when dealing with the paleoenvironmental significance of shell archives. The double PCA approach was swift and very efficient on identifying these issues, providing a new tool to screen the influence of syn- to post-depositional processes affecting sclerochronological records.

2- PCA results for all tested shell combinations

The loadings obtained for the first PCA results for all tested combinations of shell groups are summarized in Figure A6, as a complement to Figures 6 to 9 (see main text for explanations). Note similarities in elemental trend: (i) a trend towards higher Mg, Fe and Mn, opposed to lower Ca and Sr concentration presented by the control dataset as well as in all the samples representing Praia das Maçãs; a small influence of higher Si content is also detected (PC2); (ii) a main trend marked by higher Mg, Fe, Si and Al accompanied only by lowered Ca values; a minor influence of the incorporation of trace elements as Br, Pb or Zn can also be identified in shells belonging to the São Julião section; (iii) a combination of both trends described above, as obtained for the set of Pectinid shells representative of both settings (Fig. A6). The response of each site and shell-type can also be typified, depending on the species involved on each analysis and the processes dominating the elemental record (syn- to post-depositional; see Fig. 9 and main text for detailed explanations).

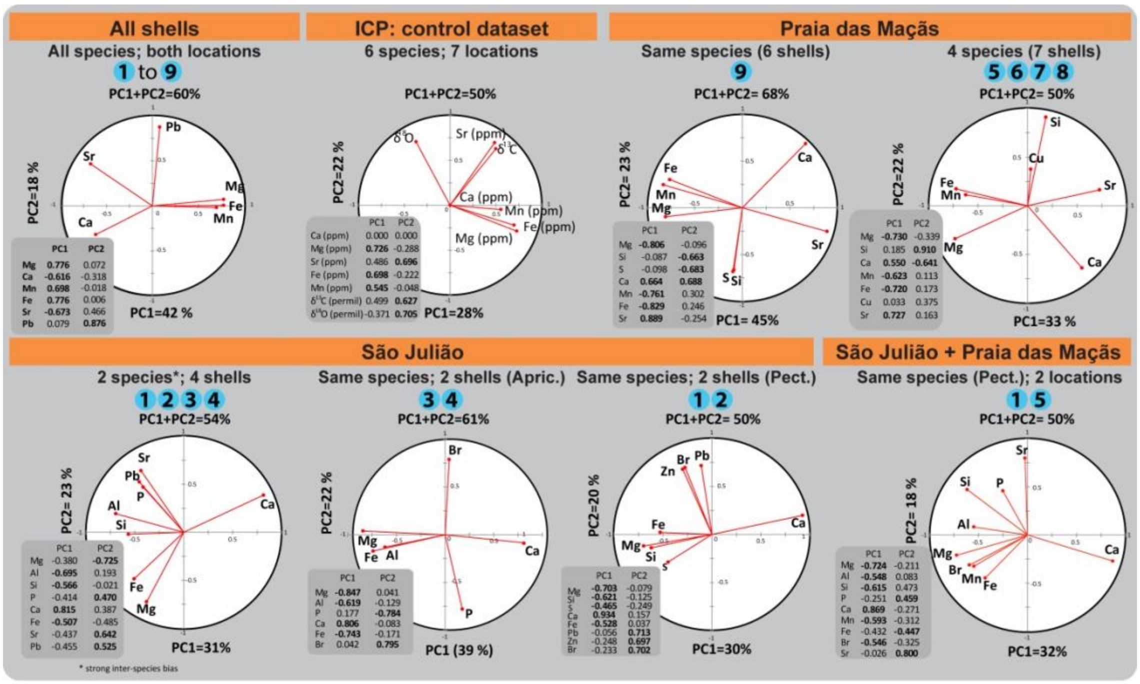

Fig. A5_Coimbra et al.

Fig. A6- Principal component loadings obtained for the tested combinations of shell data. Note that the combination of all shells is not addressed in the text. This because it resulted in largely overlapping data points along the PCA space, likely due to the high amount of information gathered in one single representation. This motivated an approach based on the combination of a lower number of shells, by location and/or by species, as described in this figure. Numeral tags (in blue) as in Figures 3 and A1.